ADAPTIVE DISCONTINUOUS GALERKIN METHODS FOR EIGENVALUE PROBLEMS ARISING IN INCOMPRESSIBLE FLUID FLOWS

K. ANDREW CLIFFE *, EDWARD J.C. HALL †, AND PAUL HOUSTON ‡

Abstract. In this article we consider the *a posteriori* error estimation and adaptive mesh refinement of discontinuous Galerkin finite element approximations of the hydrodynamic stability problem associated with the incompressible Navier–Stokes equations. Particular attention is given to the reliable error estimation of the eigenvalue problem in channel and pipe geometries. Here, computable *a posteriori* error bounds are derived based on employing the generalization of the standard Dual–Weighted–Residual approach, originally developed for the estimation of target functionals of the solution, to eigenvalue/stability problems. The underlying analysis consists of constructing both a dual eigenvalue problem and a dual problem for the original base solution. In this way, errors stemming from both the numerical approximation of the original nonlinear flow problem, as well as the underlying linear eigenvalue problem are correctly controlled. Numerical experiments highlighting the practical performance of the proposed *a posteriori* error indicator on adaptively refined computational meshes are presented.

Key words. Incompressible flows, hydrodynamic stability, *a posteriori* error estimation, adaptivity, discontinuous Galerkin methods

1. Introduction. The numerical approximation of eigenvalue problems plays a central role in the analysis of the stability of nonlinear partial differential equations. Application areas include structural mechanics and fluid mechanics; in the latter case, the terminology of hydrodynamic stability is typically used within the literature, cf. [6], for example. In this latter situation, the underlying problem will typically consist of the incompressible Navier–Stokes equations, which must be solved to compute a given base solution, coupled with an associated (linearized) eigenvalue problem; the linearization being undertaken at the computed base solution. The computation of the most dangerous or critical eigenvalue $\lambda^{\rm crit}$, namely the one with smallest real part, is of paramount importance for determining the stability of the underlying flow. Indeed, if the real part of $\lambda^{\rm crit}$ is negative, then any perturbation having a nontrivial component in the direction of the eigenfunction associated with the eigenvalue $\lambda^{\rm crit}$ may initially grow, or indeed blow up. Therefore, to understand the stability of a given system of nonlinear partial differential equations with respect to a parameter of interest, say the Reynolds number Re in the case of hydrodynamic stability, it is essential to compute both the underlying base solution and corresponding most dangerous eigenvalue to high accuracy. To undertake this task in a computationally efficient manner naturally leads to the application of adaptive mesh refinement based on rigorous *a posteriori* error estimates.

We note that if the linearized operator is far from normal, its eigenvalues may be very sensitive to small perturbations and so may be an unreliable guide to the stability of the underlying flow. See, for example, the book by Schmid and Henningson for a detailed discussion of these issues [28]. For the problems we consider in this article

* School of Mathematical Sciences, University of Nottingham, University Park, Nottingham NG7 2RD, UK, email: Andrew.Cliffe@nottingham.ac.uk.

† School of Mathematical Sciences, University of Nottingham, University Park, Nottingham NG7 2RD, UK, email: Edward.Hall@nottingham.ac.uk. The research of this author was supported by the EPSRC under grant EP/E013724/1.

‡ School of Mathematical Sciences, University of Nottingham, University Park, Nottingham NG7 2RD, UK, email: Paul.Houston@nottingham.ac.uk.

the most dangerous eigenvalues are, in fact, well conditioned and so provide reliable information concerning stability.

Over the past few decades, tremendous progress has been made in the area of *a posteriori* error estimation and adaptive finite element approximation of partial differential equations; for a review of some of the main developments in the subject we refer to the recent monographs [1, 31, 34], and the articles [16, 7]. Despite a number of significant advances in the field, much of the research to date has focused on source problems. In contrast, the development of reliable and efficient adaptive algorithms for the numerical approximation of eigenvalue problems has received considerably less attention. In the context of the finite element approximation of second–order self-adjoint elliptic eigenvalue problems we mention the recent articles [14, 15, 23, 27]; for related work, based on considering the eigenvalue problem as a parameter–dependent nonlinear equation, see Verfürth [33, 34], for example. For earlier references devoted to the derivation of *a posteriori* error bounds for the finite element approximation of symmetric eigenvalue problems, we refer to [4, 5], for example. Extensions to the finite element approximation of both the eigenvalue problem for the Stokes equations and linear elasticity may be found in the recent articles [26] and [35], respectively. Finally, we mention [19], where the convergence of an adaptive finite element method for the computation of eigenvalues and eigenfunctions of second–order self-adjoint elliptic PDEs is studied.

The treatment of non-symmetric eigenvalue problems has been considered in the article [21]; see also [6]. The approach adopted there is based on a generalization of the standard Dual–Weighted–Residual (DWR) approach, originally developed for the *a posteriori* error estimation of target functionals of the solution, to the derivation of computable bounds on the underlying eigenvalue/eigenvector of interest. The central idea involves the design of a corresponding dual eigenvalue problem to the original (primal) eigenvalue problem. By simultaneously considering the numerical approximation of the primal and dual eigenvalue problems, computable *a posteriori* error bounds on the eigenvalue of interest may be derived, under minimal regularity assumptions. For related work on the application of duality arguments in the context of *a posteriori* error estimation for source problems, we refer to [7, 22, 16, 24], and the references cited therein.

In this article we shall be concerned with the *a posteriori* error estimation and adaptive mesh refinement of discontinuous Galerkin (DG, for short) approximations of the hydrodynamic stability problem associated with the incompressible Navier–Stokes equations based on employing the generalization of the DWR approach to eigenvalue problems outlined in [6, 21]. We point out that work in this direction has been undertaken in [6, Chapter 11] for standard conforming finite element methods. However, [6, Chapter 11] only considers the estimation of the error in the underlying eigenvalue, *assuming* that the base solution has been computed sufficiently accurately. Of course, as the mesh is refined on the basis of the error in the computed eigenvalue of interest, it is natural to expect that the error in the base solution will also decrease. However, in this setting, reliable bounds on the error in the eigenvalue of interest can no longer be guaranteed. In this article, we propose an alternative approach, whereby the DWR methodology is applied to the full hydrodynamic stability problem. More precisely, we construct an augmented dual problem consisting of both a dual eigenvalue problem, together with a dual problem associated with the base problem, i.e., the incompressible Navier–Stokes system. In this manner, an *a posteriori* bound on the error in the computed eigenvalue of interest is derived, which includes both

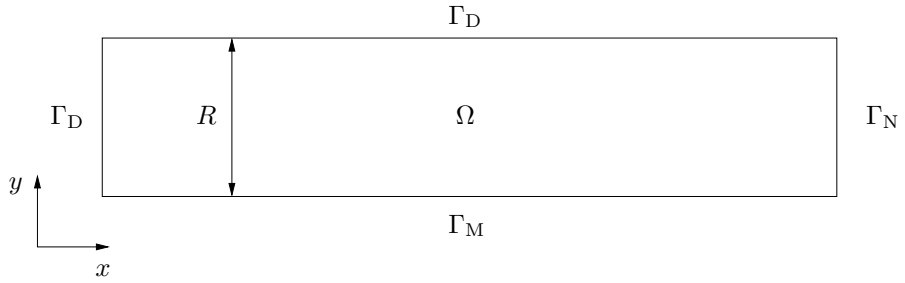

FIG. 2.1. *Generic channel domain.*

contributions arising from the error in the computed base solution, as well as the discretization error in the approximation of the linearized eigenvalue problem. By accounting for both errors in the approximation of the base solution, as well as the eigenvalue problem of interest, we shall demonstrate numerically that the effectivity indices, i.e., the ratio of the *a posteriori* error bound and the true error in the computed eigenvalue, tends to unity. In contrast, we shall also show that if the error in the base solution is neglected in the *a posteriori* error estimation, then there is a deterioration in the corresponding computed effectivities, indicating that error control can no longer be guaranteed. The emphasis of this article is the numerical approximation of the hydrodynamic stability problem for flows in channels and pipes, though we stress that the general methodology is applicable to a much wider variety of problems.

The paper is structured as follows. In Section 2 we introduce the incompressible Navier–Stokes equations and the associated eigenvalue problem resulting from their linearization about a steady–state base solution. We then introduce the DG discretization employed for the numerical approximation of the hydrodynamic stability problem, consisting of both the discretization of the base problem and the corresponding (linearized) eigenvalue problem. Then, in Section 3, we briefly recall the DWR *a posteriori* error estimation technique for the numerical approximation of general target functionals of the solution. Subsequently, we exploit this technique to derive an *a posteriori* bound for the error in the computed eigenvalue of interest which includes error contributions stemming from both the numerical approximation of the base problem, as well as the discretization of the associated eigenvalue problem. On the basis of the proposed *a posteriori* error bound, in Section 4 we investigate the practical performance of the proposed *a posteriori* error estimator on sequences of adaptively generated meshes. In particular, the quality of the (approximate) error representation formula and (approximate) *a posteriori* bound, are studied through a series of numerical experiments. Here, we consider three well documented cases: a sudden expansion in a plane channel, a channel partially blocked by a cylinder and a pipe partially blocked by a sphere. Finally, in Section 5, we summarize the work presented in this article and draw some conclusions.

2. Model problem and DG discretization. In this section we introduce mixed discontinuous Galerkin methods for the numerical approximation of both the steady incompressible Navier–Stokes equations, as well as the associated eigenvalue problem resulting from the linearization of the corresponding unsteady problem. For brevity we only consider the case of flow confined to a two–dimensional channel; the discretization of the incompressible Navier–Stokes equations in a cylindrical pipe follows analogously.

2.1. Incompressible Navier–Stokes equations. Consider the flow of an incompressible fluid confined in a generic two–dimensional channel $\Omega \in \mathbb{R}^2$ of width R with boundary $\Gamma = \Gamma_{\rm D} \cup \Gamma_{\rm N} \cup \Gamma_{\rm M}$, where $\Gamma_{\rm M}$ is parallel to the x-axis. A simple example of such a geometry is depicted in Figure 2.1, though we point out that the proceeding discussion holds for more general computational domains. Here, we impose a Dirichlet boundary condition on $\Gamma_{\rm D}$, a natural Neumann condition on $\Gamma_{\rm N}$ and a mixed Dirichlet/Neumann on $\Gamma_{\rm M}$. By introducing the Reynolds number Re, defined as $Re = Ru_{\max}/\nu$, where R is the width of the channel, $u_{\max}$ is the peak inlet velocity and ν is the kinematic viscosity, the flow can be modeled by the following non–dimensionalized unsteady Navier–Stokes equations: find $\mathbf{u} = [u_x, u_y]^\top$ and p such that

$$\frac{\partial \mathbf{u}}{\partial t} - \frac{1}{Re}\nabla^2 \mathbf{u} + (\mathbf{u}\cdot\nabla)\mathbf{u} + \nabla p = \mathbf{0}, \quad \text{in } \Omega, \tag{2.1}$$

$$\nabla \cdot \mathbf{u} = 0, \quad \text{in } \Omega, \tag{2.2}$$

with boundary conditions

$$\mathbf{u} = \mathbf{g}_{\rm D} \quad \text{on } \Gamma_{\rm D}, \tag{2.3}$$

$$\frac{1}{Re}\frac{\partial \mathbf{u}}{\partial \mathbf{n}} - p\mathbf{n} = 0 \quad \text{on } \Gamma_{\rm N}, \tag{2.4}$$

$$\frac{1}{Re}\frac{\partial u_x}{\partial \mathbf{n}} - pn_x = 0 \quad \text{and} \quad u_y = 0 \quad \text{on } \Gamma_{\rm M}, \tag{2.5}$$

subject to some appropriate initial condition. Here, $\mathbf{u}$ and p denote the velocity and pressure of the fluid, respectively, and $\mathbf{n} = (n_x, n_y)^\top$ denotes the unit outward normal vector to the boundary Γ of Ω.

In the sequel we consider the numerical approximation of the corresponding steady state problem and investigate its linear stability. With this in mind, employing the continuity equation (2.2), we rewrite the steady Navier–Stokes equations in the following divergence form (to facilitate the DG discretization): find $\mathbf{u}^0$ and p^0 such that

$$-\frac{1}{Re}\nabla^2 \mathbf{u}^0 + \nabla\cdot(\mathbf{u}^0 \otimes \mathbf{u}^0) + \nabla p^0 = \mathbf{0}, \quad \text{in } \Omega, \tag{2.6}$$

$$\nabla \cdot \mathbf{u}^0 = 0, \quad \text{in } \Omega, \tag{2.7}$$

subject to the boundary conditions outlined in (2.3)–(2.5) above, with $\mathbf{u}$ and p replaced by $\mathbf{u}^0$ and p^0, respectively. Here, for vectors $\mathbf{v} \in \mathbb{R}^m$ and $\mathbf{w} \in \mathbb{R}^n$, $m, n \geq 1$, the matrix $\mathbf{v}\otimes\mathbf{w} \in \mathbb{R}^{m\times n}$ is the standard outer product defined by $(\mathbf{v}\otimes\mathbf{w})_{kl} = v_k w_l$. For the purposes of this article, we shall refer to (2.6)–(2.7), subject to the boundary conditions (2.3)–(2.5) with $\mathbf{u}$ and p replaced by $\mathbf{u}^0$ and p^0, respectively, as the *primal base problem*; in the sequel when referring to the primal base problem (2.3)–(2.7), we shall implicitly assume that the boundary conditions (2.3)–(2.5) are enforced with $\mathbf{u}$ and p replaced by $\mathbf{u}^0$ and p^0, respectively. For ease of exposition we define the flux $\mathcal{F}^0(\cdot)$ as

$$\mathcal{F}^0(\mathbf{u}^0) := \mathbf{u}^0 \otimes \mathbf{u}^0.$$

REMARK 2.1. *The mixed boundary condition (2.5) can be viewed as a symmetry boundary condition, enabling symmetric solutions to be found in domains with reflectional symmetry about* Γ_{M} *by using only a half domain, thus saving computational time and effort. It also implicitly enforces the reflectional symmetry of the problem exactly, even in the presence of rounding errors.*

2.2. Eigenvalue problem. We shall be interested in investigating how initially small perturbations $(\delta\mathbf{u}(t), \delta p(t))$ of the steady state solution $(\mathbf{u}^0, p^0)$ behave as time evolves. With this in mind, we assume $(\mathbf{u}(t), p(t)) = (\mathbf{u}^0 + \delta\mathbf{u}, p^0 + \delta p)$, where $(\delta\mathbf{u}, \delta p)$ are of the form

$$\delta\mathbf{u} = \mathrm{e}^{-i\lambda_m t}\mathbf{u}^m,$$
$$\delta p = \mathrm{e}^{-i\lambda_m t}p^m,$$

respectively. Thereby, upon linearization of the unsteady Navier–Stokes equations (2.1)–(2.2), we obtain the following eigenvalue problem for the pair $\{\lambda^m, (\mathbf{u}^m, p^m)\}$:

$$-\frac{1}{Re}\nabla^2\mathbf{u}^m + \nabla\cdot(\mathbf{u}^m \otimes \mathbf{u}^0) + \nabla\cdot(\mathbf{u}^0 \otimes \mathbf{u}^m) + \nabla p^m = \lambda^m\mathbf{u}^m, \quad \text{in } \Omega, \tag{2.8}$$

$$-\nabla\cdot\mathbf{u}^m = 0, \quad \text{in } \Omega, \tag{2.9}$$

subject to homogeneous Dirichlet and Neumann conditions

$$\mathbf{u}^m = 0 \quad \text{on } \Gamma_{\mathrm{D}}, \tag{2.10}$$

$$\frac{1}{Re}\frac{\partial\mathbf{u}^m}{\partial\mathbf{n}} - p^m\mathbf{n} = 0 \quad \text{on } \Gamma_{\mathrm{N}}, \tag{2.11}$$

$$u_x^m = 0 \quad \text{and} \quad \frac{1}{Re}\frac{\partial u_y^m}{\partial\mathbf{n}} - p^m n_y = 0 \quad \text{on } \Gamma_{\mathrm{M}}. \tag{2.12}$$

As is customary, we also enforce the (scaling) condition $\|\mathbf{u}^m\|_0 = 1$, where $\|\cdot\|_0$ denotes the $L^2(\Omega)$–norm. We shall now refer to (2.8)–(2.12) as the *primal eigenvalue problem*. Once again, for simplicity of presentation we define the flux $\mathcal{F}^m(\cdot;\cdot)$ as

$$\mathcal{F}^m(\mathbf{u}^0;\mathbf{u}^m) := \mathbf{u}^m \otimes \mathbf{u}^0 + \mathbf{u}^0 \otimes \mathbf{u}^m.$$

REMARK 2.2. *In the application of pipe flows, the steady symmetric flow becomes unstable as the Reynolds number Re is increased, these instabilities having an antisymmetric nature. The boundary condition (2.12) can thus be viewed as an antisymmetric boundary condition, with the resultant eigenvectors being antisymmetric about* Γ_{M}*. Thus, the stability of the underlying flow can be investigated by solving the eigenvalue problem on only half of the domain, rather than the full computational domain. For further details, see, for example, [36].*

REMARK 2.3. *The linear stability of the steady state solution can then be determined by the nature of the eigenvalues* λ^m*. Standard bifurcation theory dictates that the flow is linearly stable if all eigenvalues have positive real part. Should an eigenvalue with the smallest real part be non–complex, a change of its sign from positive to negative indicates the presence of a steady bifurcation, while the crossing of a complex eigenvalue with smallest real part across the imaginary axis indicates a Hopf–bifurcation. It is therefore of fundamental importance to locate the* critical *Reynolds number at which the flow first becomes unstable.*

2.3. Meshes and traces. In this section we introduce the notation needed to define the interior penalty DG discretization of the primal base problem (2.3)–(2.7), and the primal eigenvalue problem (2.8)–(2.12).

To this end, we assume that Ω can be subdivided into shape-regular meshes $\mathcal{T}_h = \{\kappa\}$ consisting of quadrilateral elements κ. For each $\kappa \in \mathcal{T}_h$, we denote by $\mathbf{n}_\kappa$ the unit outward normal vector to the boundary $\partial\kappa$, and by h_κ the elemental diameter. An interior edge of $\mathcal{T}_h$ is the (non-empty) one-dimensional interior of $\partial\kappa^+ \cap \partial\kappa^-$, where κ^+ and κ^- are two adjacent elements of $\mathcal{T}_h$. Similarly, a boundary edge of $\mathcal{T}_h$ is the (non-empty) one-dimensional interior of $\partial\kappa \cap \Gamma$ which consists of entire edges of $\partial\kappa$. We denote by Γ_{int} the union of all interior edges of $\mathcal{T}_h$.

Next, we define average and jump operators. To this end, let κ^+ and κ^- be two adjacent elements of $\mathcal{T}_h$, and $\mathbf{x}$ be an arbitrary point on the interior edge $e = \partial\kappa^+ \cap \partial\kappa^- \subset \Gamma_{\text{int}}$. Furthermore, let q, $\mathbf{v}$, and $\underline{\tau}$ be scalar–, vector–, and matrix–valued functions, respectively, that are smooth inside each element $\kappa^\pm$. By $(q^\pm, \mathbf{v}^\pm, \underline{\tau}^\pm)$ we denote the traces of $(q, \mathbf{v}, \underline{\tau})$ on e taken from within the interior of $\kappa^\pm$, respectively. Then, we introduce the following averages at $\mathbf{x} \in e$:

$$\{\!\{q\}\!\} = (q^+ + q^-)/2, \quad \{\!\{\mathbf{v}\}\!\} = (\mathbf{v}^+ + \mathbf{v}^-)/2, \quad \{\!\{\underline{\tau}\}\!\} = (\tau^+ + \tau^-)/2.$$

Similarly, the jumps at $\mathbf{x} \in e$ are given by

$$\begin{aligned} [\![q]\!] &= q^+\mathbf{n}_{\kappa^+} + q^-\mathbf{n}_{\kappa^-}, \quad [\![\mathbf{v}]\!] = \mathbf{v}^+ \cdot \mathbf{n}_{\kappa^+} + \mathbf{v}^- \cdot \mathbf{n}_{\kappa^-}, \\ \underline{[\![\mathbf{v}]\!]} &= \mathbf{v}^+ \otimes \mathbf{n}_{\kappa^+} + \mathbf{v}^- \otimes \mathbf{n}_{\kappa^-}, \quad [\![\underline{\tau}]\!] = \underline{\tau}^+\mathbf{n}_{\kappa^+} + \underline{\tau}^-\mathbf{n}_{\kappa^-}. \end{aligned}$$

On boundary edges $e \subset \Gamma$, we set $\{\!\{q\}\!\} = q$, $\{\!\{\mathbf{v}\}\!\} = \mathbf{v}$, $\{\!\{\underline{\tau}\}\!\} = \underline{\tau}$, $[\![q]\!] = q\mathbf{n}$, $[\![\mathbf{v}]\!] = \mathbf{v} \cdot \mathbf{n}$, $\underline{[\![\mathbf{v}]\!]} = \mathbf{v} \otimes \mathbf{n}$, and $[\![\underline{\tau}]\!] = \underline{\tau}\mathbf{n}$. Here, we recall that $\mathbf{n}$ is the unit outward normal vector to the boundary Γ. For matrices $\underline{\sigma}$, $\underline{\tau} \in \mathbb{R}^{m\times n}$, $m, n \geq 1$, we use the standard notation $\underline{\sigma} : \underline{\tau} = \sum_{k=1}^{m}\sum_{l=1}^{n} \sigma_{kl}\tau_{kl}$.

2.4. Discontinuous Galerkin discretization. We now present the DG discretization employed for the numerical approximation of both the steady Navier–Stokes equations (2.3)–(2.7), and the associated eigenvalue problem (2.8)–(2.12). To this end, for a given a mesh $\mathcal{T}_h$ and polynomial degree $k \geq 1$, we introduce the following finite element spaces

$$\begin{aligned} \mathbf{V}_{h,k} &= \{\mathbf{v} \in [L^2(\Omega)]^2 : \mathbf{v}|_\kappa \in [\mathcal{Q}^k(\kappa)]^2, \kappa \in \mathcal{T}_h\}, \\ Q_{h,k} &= \{q \in L^2(\Omega) : q|_\kappa \in \mathcal{Q}^{k-1}(\kappa), \kappa \in \mathcal{T}_h\}. \end{aligned}$$

Here, $\mathcal{Q}^k(\kappa)$ denotes the space of complex multiples of tensor product polynomials on κ of degree at most k in each coordinate direction. We remark that, although solutions to (2.3)–(2.7) are real, solutions to the corresponding dual problem, cf. the next section, may be complex, as well as, of course, the solution to the associated primal and dual eigenvalue problems.

We now introduce the following symmetric version of the interior penalty method, together with a Lax–Friedrichs numerical flux approximation of the nonlinear convective terms: find $(\mathbf{u}_h^0, p_h^0) \in \mathbf{V}_{h,k} \times Q_{h,k}$ such that

$$\left\{ \begin{array}{lcl} A_h(\mathbf{u}_h^0, \bar{\mathbf{v}}_h^0) + C_h(\mathbf{u}_h^0, \bar{\mathbf{v}}_h^0) + B_h(\bar{\mathbf{v}}_h^0, p_h^0) & = & \ell_1(\bar{\mathbf{v}}_h^0), \\ B_h(\mathbf{u}_h^0, \bar{q}_h^0) & = & \ell_2(\bar{q}_h^0) \end{array} \right. \tag{2.13}$$

for all $(\mathbf{v}_h^0, q_h^0) \in \mathbf{V}_{h,k} \times Q_{h,k}$. Here, the bilinear forms A_h and B_h are defined, respectively, by

$$\begin{aligned} A_h(\mathbf{u},\mathbf{v}) = \frac{1}{\mathrm{Re}} \Bigg(& \int_\Omega \nabla_h \mathbf{u} : \nabla_h \mathbf{v} \, \mathrm{d}\mathbf{x} \\ & - \int_{\Gamma_{\mathrm{int}} \cup \Gamma_{\mathrm{D}}} (\{\!\{\nabla_h \mathbf{v}\}\!\} : \underline{[\![\mathbf{u}]\!]} + \{\!\{\nabla_h \mathbf{u}\}\!\} : \underline{[\![\mathbf{v}]\!]}) \, \mathrm{d}s \\ & - \int_{\Gamma_{\mathrm{M}}} (\{\!\{\nabla_h \mathbf{v}_y\}\!\} \cdot [\![\mathbf{u}_y]\!] + \{\!\{\nabla_h \mathbf{u}_y\}\!\} \cdot [\![\mathbf{v}_y]\!]) \, \mathrm{d}s \\ & + \int_{\Gamma_{\mathrm{int}} \cup \Gamma_{\mathrm{D}}} \sigma \underline{[\![\mathbf{u}]\!]} : \underline{[\![\mathbf{v}]\!]} \, \mathrm{d}s + \int_{\Gamma_{\mathrm{M}}} \sigma [\![\mathbf{u}_y]\!] \cdot [\![\mathbf{v}_y]\!] \, \mathrm{d}s \Bigg), \\ B_h(\mathbf{v},q) = & - \int_\Omega q \nabla_h \cdot \mathbf{v} \, \mathrm{d}\mathbf{x} + \int_{\Gamma_{\mathrm{int}} \cup \Gamma_{\mathrm{D}}} \{\!\{q\}\!\} [\![\mathbf{v}]\!] \, \mathrm{d}s \\ & + \int_{\Gamma_{\mathrm{M}}} \{\!\{q\}\!\} \mathbf{v}_y \mathbf{n}_y \, \mathrm{d}s, \end{aligned}$$

where the operator ∇_h is used to denote the broken gradient operator ∇, defined elementwise. The function $\sigma \in L^\infty(\Gamma_{\mathrm{int}} \cup \Gamma)$ is the so–called interior penalty function, which is chosen as follows: writing $\mathrm{h} \in L^\infty(\Gamma_{\mathrm{int}} \cup \Gamma)$ to denote the mesh function defined by

$$\mathrm{h}(\mathbf{x}) = \begin{cases} \min\{h_\kappa, h_{\kappa'}\}, & \mathbf{x} \in e = \partial\kappa \cap \partial\kappa' \subset \Gamma_{\mathrm{int}}, \\ h_\kappa, & \mathbf{x} \in e = \partial\kappa \cap \Gamma, \end{cases}$$

we set

$$\sigma = C_\sigma \frac{k^2}{\mathrm{h}}.$$

Here, C_σ is a positive constant which is independent of the mesh size and the polynomial degree k. To guarantee stability of the bilinear form A_h, C_σ must be chosen sufficiently large; see [3], for example, and the references cited therein.

The semilinear form C_h represents the approximation of the nonlinear convection terms and is defined by

$$\begin{aligned} C_h(\mathbf{u},\mathbf{v}) = & - \int_\Omega \mathcal{F}^0(\mathbf{u}) : \nabla_h \mathbf{v} \, \mathrm{d}\mathbf{x} + \int_{\Gamma_{\mathrm{int}}} \mathcal{H}(\mathbf{u}^+, \mathbf{u}^-, \mathbf{n}) [\![\mathbf{v}]\!] \, \mathrm{d}s \\ & + \int_\Gamma \mathcal{H}(\mathbf{u}^+, \mathbf{u}_\Gamma(\mathbf{u}^+), \mathbf{n}) [\![\mathbf{v}]\!] \, \mathrm{d}s, \end{aligned} \tag{2.14}$$

where $\mathcal{H}(\cdot,\cdot,\cdot)$ denotes the Lax-Friedrichs flux given by

$$\mathcal{H}(\mathbf{v},\mathbf{w},\mathbf{n}) := \frac{1}{2} \left(\mathcal{F}^0(\mathbf{v}) \cdot \mathbf{n} + \mathcal{F}^0(\mathbf{w}) \cdot \mathbf{n} - \alpha(\mathbf{w} - \mathbf{v}) \right).$$

Here, $\alpha := \max(\mu^+, \mu^-)$, where μ^+ and μ^- are the largest eigenvalues (in absolute magnitude) of the Jacobi matrices $(\partial/\partial\mathbf{u})(\mathcal{F}^0(\cdot)\cdot\mathbf{n})$ evaluated at $\mathbf{v}$ and $\mathbf{w}$, respectively. Thereby, in this setting, we have $\alpha = 2\max(|\mathbf{v}\cdot\mathbf{n}|, |\mathbf{w}\cdot\mathbf{n}|)$.

The boundary function $\mathbf{u}_\Gamma$ is given according to the type of boundary condition imposed. To this end, we set

$$\mathbf{u}_\Gamma(\mathbf{u}) = \mathbf{g}_{\mathrm{D}} \text{ on } \Gamma_{\mathrm{D}},$$

$$\mathbf{u}_\Gamma(\mathbf{u}) = \mathbf{u}^+ \text{ on } \Gamma_{\mathrm{N}}, \quad \mathbf{u}_\Gamma(\mathbf{u}) = [u_x^+, 0]^\top \text{ on } \Gamma_{\mathrm{M}}.$$

Finally, $\ell_1(\cdot)$ and $\ell_2(\cdot)$ are given, respectively, by

$$\begin{aligned} \ell_1(\mathbf{v}) &= -\frac{1}{Re}\int_{\Gamma_{\mathrm{D}}} ((\mathbf{g}_{\mathrm{D}} \otimes \mathbf{n}) : \nabla_h \mathbf{v} - \sigma \mathbf{g}_{\mathrm{D}} \cdot \mathbf{v})\, \mathrm{d}s, \\ \ell_2(q) &= \int_{\Gamma_{\mathrm{D}}} q \mathbf{g}_{\mathrm{D}} \cdot \mathbf{n}\, \mathrm{d}s. \end{aligned} \tag{2.15}$$

As the chosen numerical fluxes are consistent, it then follows that the underlying DG scheme is also consistent, *i.e.*, assuming sufficient regularity of the analytical solution $(\mathbf{u}^0, p^0)$, we note that

$$\left\{ \begin{array}{lcl} A_h(\mathbf{u}^0, \bar{\mathbf{v}}_h^0) + C_h(\mathbf{u}^0, \bar{\mathbf{v}}_h^0) + B_h(\bar{\mathbf{v}}_h^0, p^0) & = & \ell_1(\bar{\mathbf{v}}_h^0), \\ B_h(\mathbf{u}^0, \bar{q}_h^0) & = & \ell_2(\bar{q}_h^0) \end{array} \right. \tag{2.16}$$

for all $(\mathbf{v}_h^0, q_h^0) \in \mathbf{V}_{h,k} \times Q_{h,k}$.

Remark 2.4. *It was recently shown that, in the context of the Stokes equations, the mixed method defined above satisfies a discrete inf-sup condition, and is thereby well–posed; for details, see Hansbo and Larson [20], Toselli [32], Schötzau, Schwab and Toselli [29] and the references cited therein. We further point out that our mixed approximation in (2.13) is based on so-called mixed-order elements (or $(\mathcal{Q}^k)^2 - \mathcal{Q}^{k-1}$ elements), where the approximation degree for the pressure is of one order lower than for the velocity. In view of the approximation properties, this pair is optimally matched. However, by introducing suitable pressure stabilization terms, it is also possible to employ equal-order elements (or $(\mathcal{Q}^k)^2 - \mathcal{Q}^k$ elements) with the same approximation degree for the velocity and the pressure; see the LDG approaches by Cockburn, Kanschat, Schötzau and Schwab [13] and Cockburn, Kanschat and Schötzau [12] for details. Finally, for the treatment of the nonlinear convection terms, we refer to the article [30] where the discretization of the time–dependent incompressible Navier–Stokes equations has been undertaken.*

For the discretization of the eigenvalue problem (2.8)–(2.12), we proceed in a completely analogous fashion; here, we seek pairs $\{\lambda_h^m, (\mathbf{u}_h^m, p_h^m)\} \in \mathbb{C} \times \mathbf{V}_{h,k} \times Q_{h,k}$ such that

$$\left\{ \begin{array}{rcl} \hat{A}_h(\mathbf{u}_h^m, \mathbf{v}_h^m) + \hat{C}_h(\mathbf{u}_h^0; \mathbf{u}_h^m, \mathbf{v}_h^m) + \hat{B}_h(\bar{\mathbf{v}}_h^m, p_h^m) & = & \lambda_h^m \hat{M}(\mathbf{u}_h^m, \mathbf{v}_h^m), \\ \hat{B}_h(\mathbf{u}_h^m, \bar{q}_h^m) & = & 0, \\ \|\mathbf{u}_h^m\|_0 & = & 1 \end{array} \right. \tag{2.17}$$

for all $(\mathbf{v}_h^m, q_h^m) \in \mathbf{V}_{h,k} \times Q_{h,k}$, where, due to the anti-symmetric nature of the eigen-

functions, $\hat{A}_h$ and $\hat{B}_h$ are given, respectively, by

$$\begin{aligned}\hat{A}_h(\mathbf{u},\mathbf{v}) = \frac{1}{\mathrm{Re}}\Bigg(&\int_\Omega \nabla_h\mathbf{u} : \nabla_h\bar{\mathbf{v}}\,\mathrm{d}\mathbf{x}\\ &-\int_{\Gamma_{\mathrm{int}}\cup\Gamma_{\mathrm{D}}} (\{\!\{\nabla_h\bar{\mathbf{v}}\}\!\} : \underline{[\![\mathbf{u}]\!]} + \{\!\{\nabla_h\mathbf{u}\}\!\} : \underline{[\![\bar{\mathbf{v}}]\!]})\,\mathrm{d}s\\ &-\int_{\Gamma_{\mathrm{M}}} (\{\!\{\nabla_h\bar{\mathbf{v}}_x\}\!\}\cdot[\![\mathbf{u}_x]\!] + \{\!\{\nabla_h\mathbf{u}_x\}\!\}\cdot[\![\bar{\mathbf{v}}_x]\!])\,\mathrm{d}s\\ &+\int_{\Gamma_{\mathrm{int}}\cup\Gamma_{\mathrm{D}}} \sigma\underline{[\![\mathbf{u}]\!]} : \underline{[\![\bar{\mathbf{v}}]\!]}\,\mathrm{d}s + \int_{\Gamma_{\mathrm{M}}}\sigma[\![\mathbf{u}_x]\!]\cdot[\![\bar{\mathbf{v}}_x]\!]\,\mathrm{d}s\Bigg),\\ \hat{B}_h(\mathbf{v},q) = &-\int_\Omega q\nabla_h\cdot\mathbf{v}\,\mathrm{d}\mathbf{x} + \int_{\Gamma_{\mathrm{int}}\cup\Gamma_{\mathrm{D}}}\{\!\{q\}\!\}[\![\mathbf{v}]\!]\,\mathrm{d}s\\ &+\int_{\Gamma_{\mathrm{M}}}\{\!\{q\}\!\}\mathbf{v}_x\mathbf{n}_x\,\mathrm{d}s.\end{aligned}$$

Furthermore, $\hat{M}_h$ is defined by

$$\hat{M}_h(\mathbf{u},\mathbf{v}) := \int_\Omega \mathbf{u}\cdot\bar{\mathbf{v}}\,\mathrm{d}\mathbf{x},$$

and $\hat{C}_h$ represents the approximation of the (linear) convection terms. Employing the Lax–Friedrichs flux (or simply the upwind flux function) gives

$$\begin{aligned}\hat{C}_h(\mathbf{u}^0;\mathbf{u}^m,\mathbf{v}) = &-\int_\Omega \left(\mathcal{F}^m(\mathbf{u}^0;\mathbf{u}^m) : \nabla_h\bar{\mathbf{v}}\right)\,\mathrm{d}\mathbf{x}\\ &+\sum_{\kappa\in\mathcal{T}_h}\Bigg(\int_{\partial\kappa\setminus\Gamma}\hat{\mathcal{H}}(\{\!\{\mathbf{u}^0\}\!\};\mathbf{u}^{m,+},\mathbf{u}^{m,-},\mathbf{n})\cdot\bar{\mathbf{v}}^+\,\mathrm{d}s\\ &+\int_{\partial\kappa\cap\Gamma}\hat{\mathcal{H}}((\mathbf{u}^{0,+}+\mathbf{u}_\Gamma(\mathbf{u}^0))/2;\mathbf{u}^{m,+},\hat{\mathbf{u}}_\Gamma(\mathbf{u}^m),\mathbf{n})\cdot\bar{\mathbf{v}}^+\,\mathrm{d}s\Bigg),\end{aligned}$$

where

$$\hat{\mathcal{H}}(\mathbf{v};\mathbf{u},\mathbf{w},\mathbf{n}) := \frac{1}{2}\left(\mathcal{F}^m(\mathbf{v};\mathbf{u})\cdot\mathbf{n} + \mathcal{F}^m(\mathbf{v};\mathbf{w})\cdot\mathbf{n} + \hat{\alpha}(\mathbf{u}-\mathbf{w})\right).$$

In this case $\hat{\alpha} = |2\mathbf{v}\cdot\mathbf{n}|$, $\mathbf{u}_\Gamma$ is as before and the new boundary function $\hat{\mathbf{u}}_\Gamma$ is given by

$$\hat{\mathbf{u}}_\Gamma(\mathbf{u}) = \mathbf{0} \text{ on } \Gamma_{\mathrm{D}},$$

$$\hat{\mathbf{u}}_\Gamma(\mathbf{u}) = \mathbf{u}^+ \text{ on } \Gamma_{\mathrm{N}}, \quad \hat{\mathbf{u}}_\Gamma(\mathbf{u}) = [0, u_y^+]^\top \text{ on } \Gamma_{\mathrm{M}}.$$

Once again, the consistency of the numerical fluxes also ensures the consistency of the DG discretization. Hence, for sufficiently smooth $(\mathbf{u}^0, p^0)$ and $(\lambda^m, (\mathbf{u}^m, p^m))$, the analytical solutions of (2.3)–(2.7) and (2.8)–(2.12), respectively, we have

$$\left\{\begin{array}{rcl}\hat{A}_h(\mathbf{u}^m,\mathbf{v}_h^m) + \hat{C}_h(\mathbf{u}^0;\mathbf{u}^m,\mathbf{v}_h^m) + \hat{B}_h(\bar{\mathbf{v}}_h^m, p^m) &=& \lambda^m\hat{M}(\mathbf{u}^m,\mathbf{v}_h^m),\\ \hat{B}_h(\mathbf{u}^m,\bar{q}_h^m) &=& 0,\\ \|\mathbf{u}^m\|_0 &=& 1\end{array}\right. \tag{2.18}$$

for all $(\mathbf{v}_h^m, q_h^m) \in \mathbf{V}_{h,k}\times Q_{h,k}$.

3. A posteriori error estimation. In this section we consider the derivation of an *a posteriori* error estimate for a given eigenvalue of interest. To this end, we first recall the DWR technique in the context of error estimation for general target functionals of the solution; for further details, see [7, 22, 16, 24].

In order to proceed we first combine the base and eigenvalue discretizations defined by (2.13) and (2.17), respectively, into a single discrete system of equations. With this in mind, we wish to compute the triple $\hat{\mathbf{u}}_h := \{(\mathbf{u}_h^0, p_h^0), \lambda_h^m, (\mathbf{u}_h^m, p_h^m)\} \in (\mathbf{V}_{h,k} \times Q_{h,k}) \times \mathbb{C} \times (\mathbf{V}_{h,k} \times Q_{h,k}) := \hat{\mathbf{V}}_{h,k}$, such that

$$\mathcal{N}(\hat{\mathbf{u}}_h, \hat{\mathbf{v}}_h) = 0 \tag{3.1}$$

for all $\hat{\mathbf{v}}_h := \{(\mathbf{v}_h^0, q_h^0), \chi_h^m, (\mathbf{v}_h^m, q_h^m)\} \in \hat{\mathbf{V}}_{h,k}$, where

$$\begin{aligned}\mathcal{N}(\hat{\mathbf{u}}_h, \hat{\mathbf{v}}_h) := &-A_h(\mathbf{u}_h^0, \bar{\mathbf{v}}_h^0) - C_h(\mathbf{u}_h^0, \bar{\mathbf{v}}_h^0) - B_h(\bar{\mathbf{v}}_h^0, p_h^0) \\ &- B_h(\mathbf{u}_h^0, \bar{q}_h^0) + \ell_1(\bar{\mathbf{v}}_h^0) + \ell_2(\bar{q}_h^0) \\ &- \hat{A}_h(\mathbf{u}_h^m, \mathbf{v}_h^m) - \hat{C}_h(\mathbf{u}_h^0; \mathbf{u}_h^m, \mathbf{v}_h^m) - \hat{B}_h(\bar{\mathbf{v}}_h^m, p_h^m) - \hat{B}_h(\mathbf{u}_h^m, \bar{q}_h^m) \\ &+ \lambda_h^m \hat{M}(\mathbf{u}_h^m, \mathbf{v}_h^m) + \bar{\chi}_h^m(\|\mathbf{u}_h^m\|_0^2 - 1).\end{aligned}$$

We remark that due to the consistency of the discretization of both the primal base and eigenvalue problems, the analytical solution $\hat{\mathbf{u}} := \{(\mathbf{u}^0, p^0), \lambda^m, (\mathbf{u}^m, p^m)\}$ of (2.3)–(2.12) satisfies the consistency condition

$$\mathcal{N}(\hat{\mathbf{u}}, \hat{\mathbf{v}}_h) = 0 \qquad \forall \hat{\mathbf{v}}_h \in \hat{\mathbf{V}}_{h,k}. \tag{3.2}$$

REMARK 3.1. *To avoid the burden of extra notation we make the following remark. In the original eigenvalue problem, the bilinear form related to the approximation of the convection term, i.e., $\hat{C}_h(\cdot;\cdot,\cdot)$, is evaluated at the computed base solution $\mathbf{u}_h^0$. However, in the formulation of the augmented discretization of the full hydrodynamic stability problem, the variable $\mathbf{u}_h^0$ arising in the resulting semilinear form $\mathcal{N}(\hat{\mathbf{u}}_h, \hat{\mathbf{v}}_h)$ is assumed to not be known, but must instead be computed as part of the problem. To highlight this, it would be pertinent to modify our notation accordingly by dropping the semi-colon present in $\hat{C}_h$; for reasons of notational brevity, we retain the semi-colon notation, under the understanding that the augmented discretization (3.1) may be solved by first computing $(\mathbf{u}_h^0, p_h^0)$ followed by the evaluation of $\{\lambda_h^m, (\mathbf{u}_h^m, p_h^m)\}$.*

3.1. DWR approach for functionals. For a general target functional of practical interest $J(\cdot)$, we briefly outline the key steps involved in estimating the approximation error $J(\hat{\mathbf{u}}) - J(\hat{\mathbf{u}}_h)$ employing the DWR technique. Assuming $J(\cdot)$ is differentiable, we write $\bar{J}(\cdot,\cdot;\cdot)$ to denote the mean value linearization of $J(\cdot)$, defined by

$$\bar{J}(\hat{\mathbf{u}}, \hat{\mathbf{u}}_h; \hat{\mathbf{u}} - \hat{\mathbf{u}}_h) = J(\hat{\mathbf{u}}) - J(\hat{\mathbf{u}}_h) = \int_0^1 J'[\theta\hat{\mathbf{u}} + (1-\theta\hat{\mathbf{u}}_h)](\hat{\mathbf{u}} - \hat{\mathbf{u}}_h)\,\mathrm{d}\theta, \tag{3.3}$$

where $J'[\hat{\mathbf{w}}](\cdot)$ denotes the Fréchet derivative of $J(\cdot)$ evaluated at some $\hat{\mathbf{w}} \in \hat{\mathbf{V}}$. Here, $\hat{\mathbf{V}}$ is some suitably chosen space such that $\hat{\mathbf{V}}_{h,k} \subset \hat{\mathbf{V}}$. In the same way, we write

$$\begin{aligned}\mathcal{M}(\hat{\mathbf{u}}, \hat{\mathbf{u}}_h; \hat{\mathbf{u}} - \hat{\mathbf{u}}_h, \hat{\mathbf{w}}) &= \mathcal{N}(\hat{\mathbf{u}}, \hat{\mathbf{w}}) - \mathcal{N}(\hat{\mathbf{u}}_h, \hat{\mathbf{w}}) \\ &= \int_0^1 \mathcal{N}'_{\hat{\mathbf{u}}}[\theta\hat{\mathbf{u}} + (1-\theta)\hat{\mathbf{u}}_h](\hat{\mathbf{u}} - \hat{\mathbf{u}}_h, \hat{\mathbf{w}})\,\mathrm{d}\theta.\end{aligned} \tag{3.4}$$

We now introduce the following (formal) *dual problem*: find $\hat{\mathbf{z}} \in \hat{\mathbf{V}}$ such that

$$\mathcal{M}(\hat{\mathbf{u}}, \hat{\mathbf{u}}_h; \hat{\mathbf{w}}, \hat{\mathbf{z}}) = \bar{J}(\hat{\mathbf{u}}, \hat{\mathbf{u}}_h; \hat{\mathbf{w}}) \quad \forall \hat{\mathbf{w}} \in \hat{\mathbf{V}}. \tag{3.5}$$

We assume that (3.5) possesses a unique solution. This assumption is, of course, dependent on both the definition of $\mathcal{M}(\hat{\mathbf{u}}, \hat{\mathbf{u}}_h; \cdot, \cdot)$ and the target functional under consideration. For the proceeding error analysis, we must therefore assume that (3.5) is well–posed.

PROPOSITION 3.2 (Error Representation Formula). *Let $\hat{\mathbf{u}}$ and $\hat{\mathbf{u}}_h$ denote the solutions of (2.3)–(2.12) and (3.1), respectively, and suppose that the dual problem (3.5) is well posed, with solution $\hat{\mathbf{z}}$. Then,*

$$J(\hat{\mathbf{u}}) - J(\hat{\mathbf{u}}_h) = \varepsilon_\Omega(\hat{\mathbf{u}}, \hat{\mathbf{u}}_h; \hat{\mathbf{z}} - \hat{\mathbf{z}}_h) \equiv \sum_{\kappa \in \mathcal{T}_h} \eta_\kappa, \tag{3.6}$$

where $\eta_\kappa = \eta_\kappa^0 + \eta_\kappa^m$ with

$$\begin{aligned}
\eta_\kappa^0 = & \int_\kappa \mathbf{R}^0(\mathbf{u}_h^0, p_h^0) \cdot \bar{\mathbf{w}}^0 \, \mathrm{d}x - \frac{1}{2} \int_{\partial\kappa \setminus \Gamma} [\![p_h^0]\!] \cdot \bar{\mathbf{w}}^0 \, \mathrm{d}s + \int_{\partial\kappa \cap \Gamma_{\mathrm{N}}} \mathbf{R}_N^0(\mathbf{u}_h^0, p_h^0) \cdot \bar{\mathbf{w}}^{0,+} \, \mathrm{d}s \\
& + \int_{\partial\kappa \cap \Gamma_{\mathrm{M}}} \mathbf{R}_{M,x}^0(\mathbf{u}_h^0, p_h^0) \bar{\mathbf{w}}_x^{0,+} \, \mathrm{d}s - \frac{1}{Re} \int_{\partial\kappa \cap \Gamma_D} (\mathbf{R}_D^0(\mathbf{u}_h^0) \otimes \mathbf{n}_\kappa) : \nabla_h \bar{\mathbf{w}}^{0,+} \, \mathrm{d}s \\
& + \frac{1}{Re} \int_{\partial\kappa \cap \Gamma_D} \sigma \mathbf{R}_D^0(\mathbf{u}_h^0) \cdot \bar{\mathbf{w}}^{0,+} \, \mathrm{d}s + \frac{1}{Re} \int_{\partial\kappa \cap \Gamma_{\mathrm{M}}} \sigma \mathbf{R}_{M,y}^0(\mathbf{u}_h^0, p_h^0) \bar{\mathbf{w}}_y^{0,+} \, \mathrm{d}s \\
& - \frac{1}{Re} \int_{\partial\kappa \cap \Gamma_{\mathrm{M}}} \mathbf{R}_{M,y}^0(\mathbf{u}_h^0, p_h^0) \mathbf{n}_\kappa \cdot \nabla_h \bar{\mathbf{w}}_y^{0,+} \, \mathrm{d}s \\
& - \frac{1}{2Re} \int_{\partial\kappa \setminus \Gamma} \left\{ \underline{[\![\mathbf{u}_h^0]\!]} : \nabla_h \bar{\mathbf{w}}_h^{0,+} - [\![\nabla_h \mathbf{u}_h^0]\!] \cdot \bar{\mathbf{w}}^{0,+} \right\} \mathrm{d}s \\
& + \frac{1}{Re} \int_{\partial\kappa \setminus \Gamma} \sigma \underline{[\![\mathbf{u}_h^0]\!]} : (\bar{\mathbf{w}}^{0,+} \otimes \mathbf{n}_{\kappa^+}) + \frac{1}{2} \int_{\partial\kappa \setminus \Gamma} \bar{\omega}^{0,+} [\![\mathbf{u}_h^0]\!] \, \mathrm{d}s \\
& + \int_{\partial\kappa \cap \Gamma_{\mathrm{D}}} \bar{\omega}^{0,+} \mathbf{R}_D^0(\mathbf{u}_h^0) \cdot \mathbf{n} \, \mathrm{d}s + \int_{\partial\kappa \cap \Gamma_{\mathrm{M}}} \bar{\omega}^{0,+} \mathbf{R}_{N,x}^0(\mathbf{u}_h^0) \mathbf{n}_y \, \mathrm{d}s \\
& - \int_{\partial\kappa \setminus \Gamma} \Big(\mathcal{F}^0(\mathbf{u}_h^0) \cdot \mathbf{n}_\kappa - \mathcal{H}(\mathbf{u}_h^{0,+}, \mathbf{u}_h^{0,-}, \mathbf{n}_\kappa) \Big) \cdot \bar{\mathbf{w}}^{0,+} \, \mathrm{d}s \\
& - \int_{\partial\kappa \cap \Gamma} \Big(\mathcal{F}^0(\mathbf{u}_h^0) \cdot \mathbf{n}_\kappa - \mathcal{H}(\mathbf{u}_h^{0,+}, \mathbf{u}_\Gamma(\mathbf{u}_h^{0,+}), \mathbf{n}_\kappa) \Big) \cdot \bar{\mathbf{w}}^{0,+} \, \mathrm{d}s,
\end{aligned} \tag{3.7}$$

and $(\mathbf{w}^0, \omega^0) = (\mathbf{z}^0 - \mathbf{z}_h^0, \tau^0 - \tau_h^0)$ for all $(\mathbf{z}_h^0, \tau_h^0) \in \mathbf{V}_{h,k} \times Q_{h,k}$. Here, $\mathbf{R}^0(\mathbf{u}_h^0, p_h^0)|_\kappa = \left[\mathcal{L}^0(\mathbf{u}_h^0), \nabla_h \cdot \mathbf{u}_h^0 \right]^\top |_\kappa$ denotes the elementwise residual and $\mathbf{R}_{\mathrm{D}}^0(\mathbf{u}_h^0)$, $\mathbf{R}_{\mathrm{N}}^0(\mathbf{u}_h^0, p_h^0)$ and $\mathbf{R}_{\mathrm{M}}^0(\mathbf{u}_h^0, p_h^0)$ are the Dirichlet, Neumann and mixed boundary residuals*, respectively, given by*

$$\mathbf{R}_{\mathrm{D}}^0(\mathbf{u}_h^0)|_{\partial\kappa \cap \Gamma_{\mathrm{D}}} = (\mathbf{u}_h^+ - \mathbf{g}_{\mathrm{D}})|_{\partial\kappa \cap \Gamma_{\mathrm{in}}},$$

$$\mathbf{R}_{\mathrm{N}}^0(\mathbf{u}_h^0, p_h^0)|_{\partial\kappa \cap \Gamma_{\mathrm{N}}} = \frac{1}{Re} \frac{\partial \mathbf{u}_h^{0,+}}{\partial \mathbf{n}} - p_h^{0,+} \mathbf{n}|_{\partial\kappa \cap \Gamma_{\mathrm{N}}},$$

$$\mathbf{R}_{\mathrm{M}}^0(\mathbf{u}_h^0, p_h^0)|_{\partial\kappa \cap \Gamma_{\mathrm{M}}} = \left[\frac{1}{Re} \frac{\partial \mathbf{u}_{h,x}^{0,+}}{\partial \mathbf{n}} - p_h^{0,+} \mathbf{n}_x, \mathbf{u}_{h,y}^{0,+} \right]^\top \Bigg|_{\partial\kappa \cap \Gamma_{\mathrm{M}}}.$$

Similarly, η_κ^m is given by

$$\begin{aligned}
\eta_\kappa^m &= \int_\kappa \mathbf{R}^m(\mathbf{u}_h^0;\mathbf{u}_h^m,p_h^m)\cdot\bar{\mathbf{w}}^m\,\mathrm{d}x - \frac{1}{2}\int_{\partial\kappa\setminus\Gamma}[\![p_h^m]\!]\cdot\bar{\mathbf{w}}^m\,\mathrm{d}s + \int_{\partial\kappa\cap\Gamma_{\mathrm{N}}}\mathbf{R}_N^m(\mathbf{u}_h^m,p_h^m)\cdot\bar{\mathbf{w}}^{m,+}\,\mathrm{d}s\\
&+\int_{\partial\kappa\cap\Gamma_{\mathrm{M}}}\mathbf{R}_{M,y}^m(\mathbf{u}_h^m,p_h^m)\bar{\mathbf{w}}_y^{m,+}\,\mathrm{d}s - \frac{1}{Re}\int_{\partial\kappa\cap\Gamma_D}(\mathbf{R}_D^m(\mathbf{u}_h^m)\otimes\mathbf{n}_\kappa):\nabla_h\bar{\mathbf{w}}^{m,+}\,\mathrm{d}s\\
&+\frac{1}{Re}\int_{\partial\kappa\cap\Gamma_D}\sigma\mathbf{R}_D^m(\mathbf{u}_h^m)\cdot\bar{\mathbf{w}}^{m,+}\,\mathrm{d}s + \frac{1}{Re}\int_{\partial\kappa\cap\Gamma_{\mathrm{M}}}\sigma\mathbf{R}_{M,x}^m(\mathbf{u}_h^m,p_h^m)\bar{\mathbf{w}}_x^{0,+}\,\mathrm{d}s\\
&-\frac{1}{Re}\int_{\partial\kappa\cap\Gamma_{\mathrm{M}}}\mathbf{R}_{M,x}^0(\mathbf{u}_h^m,p_h^m)\mathbf{n}_\kappa\cdot\nabla_h\bar{\mathbf{w}}_x^{m,+}\,\mathrm{d}s\\
&-\frac{1}{2Re}\int_{\partial\kappa\setminus\Gamma}\left\{\underline{[\![\mathbf{u}_h^m]\!]}:\nabla_h\bar{\mathbf{w}}^{m,+} - [\![\nabla_h\mathbf{u}_h^m]\!]\cdot\bar{\mathbf{w}}^{m,+}\right\}\mathrm{d}s\\
&+\frac{1}{Re}\int_{\partial\kappa\setminus\Gamma}\sigma\underline{[\![\mathbf{u}_h^m]\!]}:(\bar{\mathbf{w}}^{m,+}\otimes\mathbf{n}_\kappa)\,\mathrm{d}s + \frac{1}{2}\int_{\partial\kappa\setminus\Gamma}\bar{\omega}^{m,+}[\![\mathbf{u}_h^m]\!]\,\mathrm{d}s\\
&+\int_{\partial\kappa\cap\Gamma_{\mathrm{D}}}\bar{\omega}^{m,+}\mathbf{R}_D^m(\mathbf{u}_h^m)\cdot\mathbf{n}\,\mathrm{d}s + \int_{\partial\kappa\cap\Gamma_{\mathrm{M}}}\bar{\omega}^{m,+}\mathbf{R}_{M,x}^m(\mathbf{u}_h^m)\mathbf{n}_x\,\mathrm{d}s\\
&-\int_{\partial\kappa\setminus\Gamma}\left(\mathcal{F}^m(\mathbf{u}_h^0;\mathbf{u}_h^m)\cdot\mathbf{n}_\kappa - \hat{\mathcal{H}}(\{\!\{\mathbf{u}_h^0\}\!\};\mathbf{u}^{m,+},\mathbf{u}^{m,-},\mathbf{n})\right)\cdot\bar{\mathbf{w}}^{m,+}\,\mathrm{d}s\\
&-\int_{\partial\kappa\cap\Gamma}\left(\mathcal{F}^m(\mathbf{u}_h^0;\mathbf{u}_h^m)\cdot\mathbf{n}_\kappa - \hat{\mathcal{H}}((\mathbf{u}^{0,+}+\mathbf{u}_\Gamma(\mathbf{u}^0))/2;\mathbf{u}^{m,+},\hat{\mathbf{u}}_\Gamma(\mathbf{u}^m),\mathbf{n})\right)\cdot\bar{\mathbf{w}}^{m,+}\,\mathrm{d}s
\end{aligned}$$

and $(\mathbf{w}^m,\omega^m) = (\mathbf{z}^m-\mathbf{z}_h^m,\tau^m-\tau_h^m)$ for all $(\mathbf{z}_h^m,\tau_h^m)\in\mathbf{V}_{h,k}\times Q_{h,k}$. Here, we write $\mathbf{R}^m(\mathbf{u}_h^0;\mathbf{u}_h^m,p_h^m)|_\kappa = \left[\mathcal{L}^m(\mathbf{u}_h^0;\mathbf{u}_h^m,p_h^m) - \lambda^m\mathbf{u}_h^m,\nabla_h\cdot\mathbf{u}_h^m\right]^\top|_\kappa$ to denote the elementwise residual and $\mathbf{R}_{\mathrm{D}}^m(\mathbf{u}_h^m)$, $\mathbf{R}_{\mathrm{N}}^m(\mathbf{u}_h^m,p_h^m)$ and $\mathbf{R}_{\mathrm{M}}^m(\mathbf{u}_h^m,p_h^m)$ are the Dirichlet, Neumann and mixed boundary residuals *of the eigenfunctions, respectively, given by*

$$\mathbf{R}_{\mathrm{D}}^m(\mathbf{u}_h^m)|_{\partial\kappa\cap\Gamma_{\mathrm{D}}} = \mathbf{u}_h^+|_{\partial\kappa\cap\Gamma_{\mathrm{D}}},$$

$$\mathbf{R}_{\mathrm{N}}^m(\mathbf{u}_h^m,p_h^m)|_{\partial\kappa\cap\Gamma_{\mathrm{N}}} = \frac{1}{Re}\frac{\partial\mathbf{u}_h^{m,+}}{\partial\mathbf{n}} - p_h^{m,+}\mathbf{n}|_{\partial\kappa\cap\Gamma_{\mathrm{N}}},$$

$$\mathbf{R}_{\mathrm{M}}^m(\mathbf{u}_h^m,p_h^m)|_{\partial\kappa\cap\Gamma_{\mathrm{M}}} = \left[\mathbf{u}_{h,x}^{m,+},\frac{1}{Re}\frac{\partial\mathbf{u}_{h,y}^{m,+}}{\partial\mathbf{n}} - p_h^{m,+}\mathbf{n}_y\right]^\top\Bigg|_{\partial\kappa\cap\Gamma_{\mathrm{M}}}.$$

Proof. Upon choosing $\hat{\mathbf{w}} = \hat{\mathbf{u}} - \hat{\mathbf{u}}_h$ in (3.5), recalling the linearization performed in (3.3) and (3.4) and exploiting the consistency of the DG discretizations (2.16) and (2.18) we have

$$\begin{aligned}
J(\hat{\mathbf{u}}) - J(\hat{\mathbf{u}}_h) &= \bar{J}(\hat{\mathbf{u}},\hat{\mathbf{u}}_h;\hat{\mathbf{u}}-\hat{\mathbf{u}}_h) = \mathcal{M}(\hat{\mathbf{u}},\hat{\mathbf{u}}_h;\hat{\mathbf{u}}-\hat{\mathbf{u}}_h,\hat{\mathbf{z}})\\
&= \mathcal{M}(\hat{\mathbf{u}},\hat{\mathbf{u}}_h;\hat{\mathbf{u}}-\hat{\mathbf{u}}_h,\hat{\mathbf{z}}-\hat{\mathbf{z}}_h) = -\mathcal{N}(\hat{\mathbf{u}}_h,\hat{\mathbf{z}}-\hat{\mathbf{z}}_h)\quad\forall\hat{\mathbf{z}}_h\in\hat{\mathbf{V}}_{h,k}.
\end{aligned}$$

Equation (3.6) then follows by application of the integration by parts formula. ∎

Corollary 3.3 (Type I error bound). *Given that the assumptions of Proposition 3.2 hold, then*

$$|J(\hat{\mathbf{u}}) - J(\hat{\mathbf{u}}_h)| \le \sum_{\kappa\in\mathcal{T}_h}|\eta_\kappa|, \tag{3.8}$$

where η_κ is as given in Proposition 3.2.

Proof. Equation (3.8) follows from (3.6) by use of the triangle inequality. □

REMARK 3.4. *We note that the elemental error indicators η_κ, $\kappa \in \mathcal{T}_h$, consist of two parts: η_κ^0 and η_κ^m. The former indicator can be employed to estimate the contribution to the overall error stemming from the DG approximation of the primal base problem, while the latter indicator measures the local contribution to the error committed in the approximation of the underlying primal eigenvalue problem.*

3.2. *A posteriori* error estimation for eigenvalues. In order to exploit the above analysis for the estimation of the error in a given eigenvalue λ^m of interest, we proceed as in Heuveline & Rannacher [21]. More precisely, we reformulate the evaluation of the eigenvalue λ^m as the estimation of a nonlinear target functional of the solution. To this end, following [21], the functional of interest may be defined by

$$J(\hat{\mathbf{v}}) := \chi^m \|\mathbf{v}^m\|_0^2, \tag{3.9}$$

in which case

$$J(\hat{\mathbf{u}}) - J(\hat{\mathbf{u}}_h) = \lambda^m - \lambda_h^m,$$

by virtue of the fact that $\|\mathbf{u}^m\|_0 = 1$ and $\|\mathbf{u}_h^m\|_0 = 1$.

REMARK 3.5. *We remark that the choice of the definition of the functional (3.9) is not unique. Indeed, one may simply select $J(\cdot)$ as $J(\hat{\mathbf{v}}) := \chi^m$, in which case the resultant dual problem has complex coefficients and requires the solution of one extra equation. As we shall see below, the functional defined in (3.9) leads to a more natural dual problem which consists of a dual eigenvalue problem and a dual base problem, thus mirroring the original problem. It is worth pointing out that numerical experiments indicate that the resulting error indicators using either of these definitions for $J(\cdot)$ lead to almost identical results. However, the latter definition is more pertinent in the context of parameter estimation in bifurcation problems; see, for example, [9].*

3.3. Numerical approximation of the dual problem. With $J(\cdot)$ defined by (3.9), we now proceed to formulate the dual problem. For $\hat{\mathbf{z}} = \{(\mathbf{z}^0, \tau^0), \mu^m, (\mathbf{z}^m, \tau^m)\}$ we calculate the Fréchet derivative of $\mathcal{N}(\cdot, \hat{\mathbf{z}})$ in the direction $\hat{\mathbf{v}}$ at a fixed point $\hat{\mathbf{u}}$, i.e.,

$$\begin{aligned}
\mathcal{N}'_{\hat{\mathbf{u}}}[\hat{\mathbf{u}}](\hat{\mathbf{v}}, \hat{\mathbf{z}}) = &-A_h(\mathbf{v}^0, \bar{\mathbf{z}}^0) - C'_h[\mathbf{u}^0](\mathbf{v}^0, \bar{\mathbf{z}}^0) - B_h(\bar{\mathbf{z}}^0, q^0) - B_h(\mathbf{v}^0, \bar{\tau}^0) \\
&-\hat{A}_h(\mathbf{v}^m, \mathbf{z}_h^m) - \hat{B}_h(\bar{\mathbf{z}}^m, q^m) - \hat{B}_h(\mathbf{v}^m, \bar{\tau}^m) \\
&-\hat{C}_h(\mathbf{u}^0; \mathbf{v}^m, \mathbf{z}^m) - \hat{C}_h(\mathbf{v}^0; \mathbf{z}^m, \mathbf{u}^m) + \chi^m(\mathbf{u}^m, \mathbf{z}^m) \\
&+\lambda^m(\mathbf{v}^m, \mathbf{z}^m) + 2\bar{\mu}^m \mathrm{Re}(\mathbf{u}^m, \mathbf{v}^m),
\end{aligned}$$

where

$$\begin{aligned}
C'_h[\mathbf{u}^0](\mathbf{v}^0, \mathbf{z}^0) = &-\int_\Omega (\mathbf{u}^0 \otimes \mathbf{v}^0) : \nabla_h \mathbf{z}^0 \,\mathrm{d}\mathbf{x} - \int_\Omega (\mathbf{v}^0 \otimes \mathbf{u}^0) : \nabla_h \mathbf{z}^0 \,\mathrm{d}\mathbf{x} \\
&+ \int_{\partial\kappa \setminus \Gamma} \mathcal{H}'[\mathbf{u}^0](\mathbf{v}^{0,+}, \mathbf{v}^{0,-}, \mathbf{n}) \cdot \mathbf{z}^0 \,\mathrm{d}s \\
&+ \int_{\partial\kappa \cap \Gamma} \mathcal{H}'[\mathbf{u}^0](\mathbf{v}^{0,+}, \mathbf{u}_\Gamma(\mathbf{v}_h^0), \mathbf{n}) \cdot \mathbf{z}^0 \,\mathrm{d}s.
\end{aligned}$$

Similarly, the Fréchet derivative of $J(\cdot)$ in the direction $\hat{\mathbf{v}}$ at a fixed point $\hat{\mathbf{u}}$ is

$$J'[\hat{\mathbf{u}}](\hat{\mathbf{v}}) = \chi^m \|\mathbf{u}^m\|_0^2 + 2\lambda^m \mathrm{Re}(\mathbf{u}^m, \mathbf{v}^m).$$

Rather than linearizing about $\mathbf{u} - \mathbf{u}_h$, we simply consider the linearization about just $\mathbf{u}$; in practice, this linearization will be performed on the basis of the current numerical solution. Thereby, we have the resultant (approximate) dual problem: find $\hat{\mathbf{z}} = (\mathbf{z}^0, \tau^0), \mu^m, (\mathbf{z}^m, \tau^m))$ such that

$$\begin{aligned}
&-A_h(\mathbf{v}^0, \bar{\mathbf{z}}^0) - C_h'[\mathbf{u}^0](\mathbf{v}^0, \bar{\mathbf{z}}^0) - B_h(\bar{\mathbf{z}}^0, q^0) \\
&- B_h(\mathbf{v}^0, \bar{\tau}^0) - \hat{A}_h(\mathbf{v}^m, \mathbf{z}^m) - \hat{B}_h(\bar{\mathbf{z}}^m, q^m) \\
&- \hat{B}_h(\mathbf{v}^m, \bar{\tau}^m) - \hat{C}_h(\mathbf{u}^0; \mathbf{v}^m, \mathbf{z}^m) - \hat{C}_h(\mathbf{v}^0; \mathbf{u}^m, \mathbf{z}^m) \\
&+ \chi^m(\mathbf{u}^m, \mathbf{z}^m) + \lambda^m(\mathbf{v}^m, \mathbf{z}^m) + 2\bar{\mu}^m \mathrm{Re}(\mathbf{u}^m, \mathbf{v}^m) = \\
&\qquad \chi^m \|\mathbf{u}^m\|_0^2 + 2\lambda^m \mathrm{Re}(\mathbf{u}^m, \mathbf{v}^m) \quad \forall \hat{\mathbf{v}} \in \hat{\mathbf{V}}. \qquad (3.10)
\end{aligned}$$

By a process of back substitution, we see that the solution to (3.10) can be found by first solving a *dual eigenvalue problem* and substituting the result back into a *dual base problem*. Hence, the dual eigenvalue problem becomes: find the pair $(\mu^m, (\mathbf{z}^m, \tau^m)) \in \mathbb{C} \times \mathbf{V}$ such that

$$\begin{aligned}
&-\hat{A}_h(\mathbf{v}^m, \mathbf{z}^m) - \hat{B}_h(\bar{\mathbf{z}}^m, q^m) - \hat{B}_h(\mathbf{v}^m, \bar{\tau}^m) - \hat{C}_h(\mathbf{u}^0; \mathbf{v}^m, \mathbf{z}^m) \\
&\qquad + \chi^m(\mathbf{u}^m, \mathbf{z}^m) + \lambda^m(\mathbf{v}^m, \mathbf{z}^m) + 2\bar{\mu}^m \mathrm{Re}(\mathbf{u}^m, \mathbf{v}^m) = \\
&\qquad\qquad \chi^m \|\mathbf{u}^m\|_0^2 + 2\lambda^m \mathrm{Re}(\mathbf{u}^m, \mathbf{v}^m) \quad \forall \hat{\mathbf{v}} \in \hat{\mathbf{V}}^m. \qquad (3.11)
\end{aligned}$$

However, it is perhaps more natural to consider the alternative dual eigenvalue problem: find $(\tilde{\mu}^m, (\tilde{\mathbf{z}}^m, \tilde{t}^m)) \in \hat{\mathbf{V}}^m$ such that

$$\begin{aligned}
\hat{A}_h(\mathbf{v}^m, \tilde{\mathbf{z}}^m) + \hat{B}_h(\mathbf{v}^m, \bar{\tilde{t}}^m) + \hat{C}_h(\mathbf{u}_h^0; \mathbf{v}^m, \tilde{\mathbf{z}}^m) &= \tilde{\mu}^m(\mathbf{v}^m, \tilde{\mathbf{z}}^m), \\
\hat{B}_h(\bar{\tilde{\mathbf{z}}}^m, q^m) = 0 \quad \forall \hat{\mathbf{v}} \in \hat{\mathbf{V}}^m, \qquad (3.12)
\end{aligned}$$

subject to the scaling condition $(\mathbf{u}^m, \tilde{\mathbf{z}}^m) = 1$. Indeed, it follows directly that $\tilde{\mu}^m = \bar{\lambda}^m$, and hence, $(\tilde{\mu}^m, (\tilde{\mathbf{z}}^m, \tilde{t}^m))$ is also the solution of (3.11).

Finally, the dual base solution becomes: find $(\mathbf{z}^0, \tau^0) \in \hat{\mathbf{V}}^0$ such that

$$\begin{aligned}
&A_h(\mathbf{v}^0, \bar{\mathbf{z}}^0) + C_h'[\mathbf{u}^0](\mathbf{v}^0, \bar{\mathbf{z}}^0) + B_h(\bar{\mathbf{z}}^0, q^0) \\
&\qquad + B_h(\mathbf{v}^0, \bar{\tau}^0) = \hat{C}_h(\mathbf{v}^0; \mathbf{u}^m, \mathbf{z}^m) \quad \forall \mathbf{v}^0 \in \hat{\mathbf{V}}^0. \qquad (3.13)
\end{aligned}$$

Thus, the dual base solution is dependent on the primal base solution and both the dual and primal eigenfunctions and, as such, in the case of complex eigenvalues is also complex.

In order to approximate (3.12) and (3.13) numerically, we now proceed by replacing $\hat{\mathbf{u}}$ with $\hat{\mathbf{u}}_h$ and seeking a discrete alternative $\hat{\mathbf{z}}_h$ to $\hat{\mathbf{z}}$. Evidently, seeking $\hat{\mathbf{z}}_h \in \hat{\mathbf{V}}_{h,k}$ is not applicable as, by virtue of (3.1), our error estimate would be identically zero. Instead we seek $\hat{\mathbf{z}}_h$ computed on the same mesh $\mathcal{T}_h$ used for $\hat{\mathbf{u}}_h$, but with a higher degree polynomial. Thus, our discrete dual eigenvalue problem becomes: find $\{\mu_h^m, (\mathbf{z}_h^m, \tau_h^m)\} \in \mathbb{C} \times (\mathbf{V}_{h,\hat{k}} \times Q_{h,\hat{k}})$ such that

$$\begin{aligned}
\hat{A}_h(\mathbf{v}_h^m, \mathbf{z}_h^m) + \hat{B}_h(\mathbf{v}_h^m, \bar{\tau}_h^m) + \hat{C}_h(\mathbf{u}_h^0; \mathbf{v}_h^m, \mathbf{z}_h^m) &= \mu_h^m(\mathbf{v}_h^m, \mathbf{z}_h^m), \\
\hat{B}_h(\bar{\mathbf{z}}_h^m, q_h^m) = 0 \qquad (3.14)
\end{aligned}$$

for all $(\mathbf{v}_h^m, q_h^m) \in \mathbf{V}_{h,\hat{k}} \times Q_{h,\hat{k}}$, with $(\mathbf{u}_h^m, \tilde{\mathbf{z}}_h^m) = 1$, where $\hat{k} > k$. Similarly, the discrete dual base problem becomes: find $(\mathbf{z}_h^0, \tau_h^0) \in \mathbf{V}_{h,\hat{k}} \times Q_{h,\hat{k}}$ such that

$$\begin{aligned}
&A_h(\mathbf{v}_h^0, \bar{\mathbf{z}}_h^0) + C_h'[\mathbf{u}_h^0](\mathbf{v}_h^0, \bar{\mathbf{z}}_h^0) + B_h(\bar{\mathbf{z}}_h^0, q_h^0) \\
&\qquad + B_h(\mathbf{v}_h^0, \bar{\tau}_h^0) = \hat{C}_h(\mathbf{v}_h^0; \mathbf{u}_h^m, \mathbf{z}_h^m) \qquad (3.15)
\end{aligned}$$

for all $(\mathbf{v}_h^0, q_h^0) \in \mathbf{V}_{h,\hat{k}} \times Q_{h,\hat{k}}$, Hence, we have the following approximate *a posteriori* error bound

$$|\lambda^m - \lambda_h^m| \lesssim \sum_{\kappa \in \mathcal{T}_h} |\hat{\eta}_\kappa|,$$

where $\hat{\eta}_\kappa$ is defined in an analogous manner to η_κ, cf. Proposition 3.2, with $\hat{\mathbf{z}}$ replaced by $\hat{\mathbf{z}}_h$.

REMARK 3.6. *Although not of interest for our current applications, we point out that the same general framework may be employed to control the error in certain target functionals of the eigenfunctions; see Heuveline and Rannacher [21] for details.*

4. Numerical experiments. In this section we present a series of numerical examples to demonstrate the practical performance of the proposed *a posteriori* error estimator derived in Proposition 3.2 within an automatic adaptive refinement procedure which is based on 1-irregular quadrilateral elements; i.e., elements which contain at most one hanging node per element-edge, which we assume to be the barycenter of the edge. Here, the elements are marked for refinement/derefinement on the basis of the size of the elemental error indicators $|\hat{\eta}_\kappa|$ using the fixed fraction refinement algorithm with refinement and derefinement fractions set to 25% and 10%, respectively. In each of the examples shown in this section, we set $C_\sigma = 10$, $k = 2$, and $\hat{k} = 3$. The resulting system of nonlinear equations arising in the numerical approximation of the primal base solution are solved by a damped Newton method; within each inner (linear) iteration, we exploit the MUltifrontal Massively Parallel Solver (MUMPS), see [2] for details. However, we point out that for high Reynolds numbers it is necessary to employ a continuation technique based on computing approximations at lower Reynolds numbers initially, before increasing Re to the desired value.

The discretization of the primal and dual eigenvalue problems require the computation of the eigenvalue with smallest real part satisfying a system of the form

$$A\mathbf{x} = \lambda B\mathbf{x}, \tag{4.1}$$

where, with an abuse of notation, A, B, and $\mathbf{x}$ take the form

$$A = \begin{bmatrix} K & C \\ C^\top & 0 \end{bmatrix}, \quad B = \begin{bmatrix} M & 0 \\ 0 & 0 \end{bmatrix}, \quad \text{and} \quad \mathbf{x} = \begin{pmatrix} \mathbf{u} \\ \mathbf{p} \end{pmatrix}. \tag{4.2}$$

In order to solve (4.1) we employ the Arnoldi Package (ARPACK) of Lehoucq, Sorensen and Yang [25]. We point out that ARPACK is most adept at finding highly separated eigenvalues with large magnitude, and not necessarily those with small real part that determine linear stability. Another issue is that, due to the mass matrix having a zero diagonal block, there are a number of infinite eigenvalues, which we wish to avoid computing. To overcome these difficulties, Cliffe *et* al. [8] proposed the use of a modified Cayley transform to compute the solution of (4.1). This involves solving a modified eigenvalue problem of the form

$$\begin{bmatrix} K - \mu M & \beta C \\ \beta C^\top & 0 \end{bmatrix} \begin{pmatrix} \mathbf{u} \\ \mathbf{q} \end{pmatrix} = \theta \begin{bmatrix} K - \sigma M & C \\ C^\top & 0 \end{bmatrix} \begin{pmatrix} \mathbf{u} \\ \mathbf{q} \end{pmatrix}, \tag{4.3}$$

where $\sigma < \mu$ and β are real–valued parameters. Under this transformation it is readily shown, see Garratt [18], that for finite eigenvalues

$$\theta = \frac{\lambda - \mu}{\lambda - \sigma} \quad \text{and} \quad \mathbf{q} = \frac{(\theta - 1)\mathbf{p}}{\theta - \beta}, \tag{4.4}$$

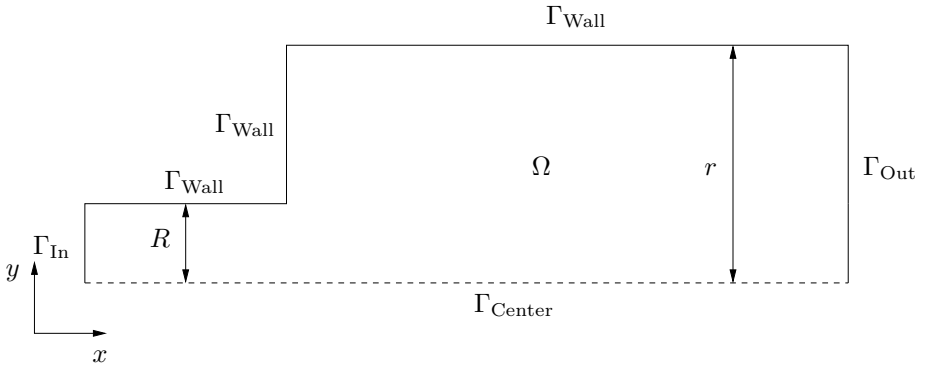

FIG. 4.1. *Example 1: Half Channel with a Sudden Expansion*

while the infinite eigenvalues are mapped to β. Furthermore,

$$\text{Re}(\lambda) < \frac{1}{2}(\sigma + \mu) \Leftrightarrow |\theta| > 1,$$
$$\text{Re}(\lambda) \geq \frac{1}{2}(\sigma + \mu) \Leftrightarrow |\theta| \leq 1;$$

hence, by choosing σ and μ in a judicious manner and selecting $\beta = 0$ we can ensure the computation of the eigenvalue of interest. Solution by ARPACK of (4.3) involves the repeated multiplication of a vector by the inverse of

$$\begin{bmatrix} K - \sigma M & C \\ C^{\top} & 0 \end{bmatrix}. \tag{4.5}$$

For computational efficiency, we again employ the MUMPS [2] direct matrix solver which computes and stores the factors of (4.5).

4.1. Example 1. In this first example we consider the flow in a channel with a sudden expansion; the ratio of the half-width of expanded section of the channel, r, to that of the inlet section channel, R, being set to 3:1 and the outlet being sufficiently long to allow Poiseuille flow to have fully developed at the exit, see Figure 4.1. On entry, Γ_{in}, the flow is also assumed to be Poiseuille; no slip Dirichlet conditions are imposed on Γ_{Wall}, a Neumann condition is enforced on Γ_{Out} and the mixed boundary condition is imposed on Γ_{center}. In this situation it is well known, see [17], that at around $Re = 40$ there is a steady symmetry breaking bifurcation, where a real eigenvalue crosses the imaginary axis. As such, we explore the eigenvalue error estimation and mesh adaptivity near to this bifurcation point by setting $Re = 35$. In this case the eigenvalue with smallest real part has true value 0.00613553131999. We begin with a uniform starting grid, comprising 760 elements and perform 6 adaptive refinement steps based on employing the fixed fraction refinement strategy.

Table 4.1 shows the number of elements, the number of degrees of freedom for both the primal base and primal eigenvalue problems, the error in the eigenvalue and the error effectivities when the full indicator $|\sum_{\kappa\in\mathcal{T}_h} \hat{\eta}_\kappa|$ is used and when the partial indicator $|\sum_{\kappa\in\mathcal{T}_h} \hat{\eta}^m_\kappa|$, based only on computing the error in the eigenvalue alone, cf. [6], are employed. We first notice that the effectivities when using the full error indicator tend towards unity as the mesh is refined indicating that as the adaptive algorithm proceeds, a reliable prediction of the error in the computed eigenvalue of

Mesh No	No. Eles	Base DOF	Eig. Dof	$\lvert\lambda - \lambda_h\rvert$	$\lvert\sum_{\kappa\in\mathcal{T}_h} \hat{\eta}_\kappa\rvert$	$\lvert\sum_{\kappa\in\mathcal{T}_h} \hat{\eta}^m_\kappa\rvert$
1	760	16720	16720	6.027E-05	1.92	0.14
2	1387	30514	30514	1.540E-05	2.47	0.96
3	2479	54538	54538	9.795E-06	1.98	1.16
4	4387	96514	96514	6.327E-06	1.58	0.98
5	7645	168190	168190	3.845E-06	1.33	0.80
6	13243	291346	291346	2.231E-06	1.16	0.67
7	22585	496870	496870	1.281E-06	1.00	0.56

TABLE 4.1
Example 1: Adaptive algorithm for $Re = 35$.

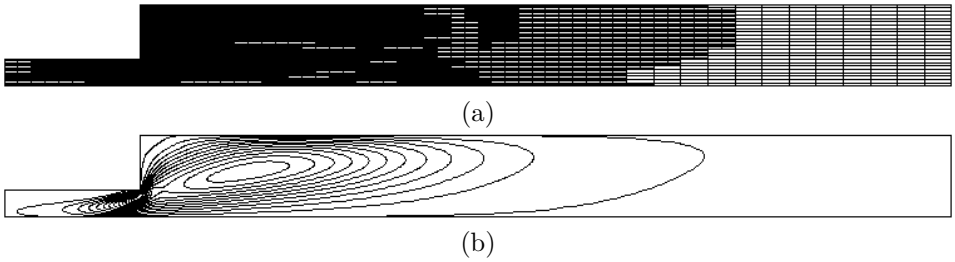

FIG. 4.2. *Example 1: (a) Mesh after 5 refinement steps, (b) Contour plot of $\mathbf{z}^m_x$.*

interest may be determined. In contrast, the effectivities when using only the partial error indicator seem to be extremely unreliable; for this example, we observe around a 50% underestimation of the error on the final mesh.

Figures 4.2(a) and 4.3(a) show the mesh after 5 and 6 refinement steps, respectively; the latter shows the detail of the mesh in the vicinity of the expansion point. Indeed, from Figure 4.3(a) we observe that the majority of the refinement has been performed around the reentrant corner. For brevity we do not show plots of all the components of the primal base and dual solution and primal and dual eigenfunctions; instead, we show contour plots of the x–component of the dual eigenvector and the y–component of the dual base solution in Figures 4.2(b) and 4.3(b), respectively, in order to indicate how the refinement has been directed towards the structure in the dual solutions.

Finally, in Figure 4.4 we compare the performance of the adaptive mesh refinement strategy against a uniform refinement strategy; here the error in the computed eigenvalue is plotted against the number of degrees of freedom (in the primal eigenvalue problem) for the both strategies. The superiority of the adaptive refinement algorithm is evident: for a given number of degrees of freedom the error in the eigenvalue computed on the adaptively refined meshes is always less than the corresponding quantity computed using simply uniform refinement of the mesh. Indeed, on the final grid, for the same number of degrees of freedom the adaptive strategy leads to almost an order of magnitude improvement in error $|\lambda - \lambda_h|$ in comparison with the uniform mesh refinement strategy.

4.2. Example 2. In this second example we consider flow in a channel with a cylinder centered on the midline of the channel partially blocking the flow; the radius of the cylinder is r and the half-width of the channel is R, see Figure 4.5. We consider a blockage ratio $r : R = 1 : 2$, with Poiseuille flow on entry, no slip

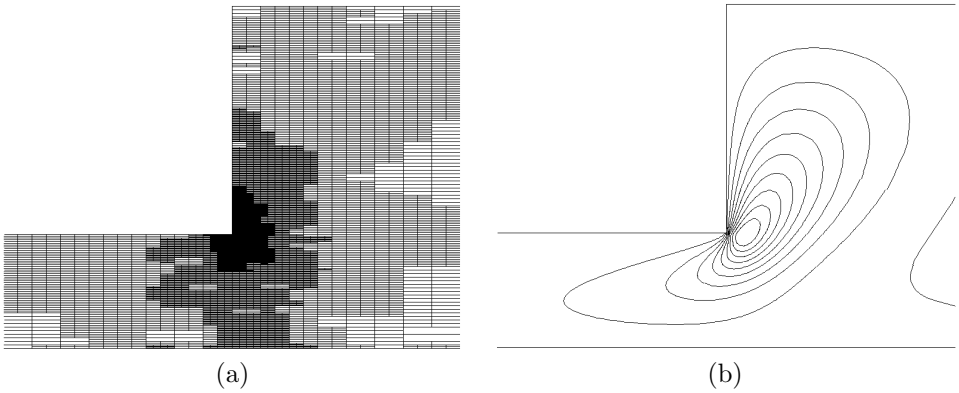

FIG. 4.3. *Example 1: (a) Mesh detail near expansion, (b) Contour plot of* $\mathbf{z}_y$ *near expansion.*

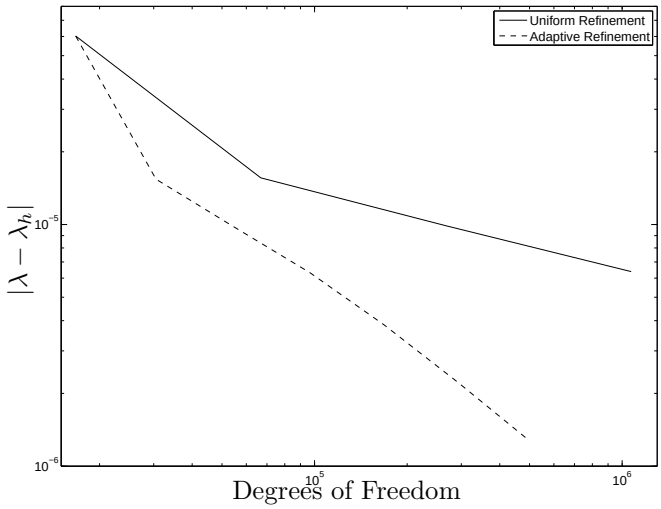

FIG. 4.4. *Example 1: Error Convergence*

conditions on Γ_{Wall} and Γ_{B}, a Neumann condition on Γ_{Out} and a mixed condition on Γ_{Center}. For this configuration a Hopf bifurcation occurs at around $Re \approx 120$, see [11]. Here, we set $Re = 100$ and seek to perform error estimation and adaptivity for the eigenvalue with the smallest real part; the true value of this eigenvalue is $0.114789963956350 + 2.116719676204527i$. Our starting grid has 816 elements and is fitted around the blockage.

As before, we show in tabular form the number of elements, the number of degrees of freedom for both the primal base and primal eigenvalue problems, the error in the eigenvalue and the error effectivities when the full indicator $|\sum_{\kappa\in\mathcal{T}_h}\hat{\eta}_\kappa|$ is used and when the partial indicator $|\sum_{\kappa\in\mathcal{T}_h}\hat{\eta}^m_\kappa|$, based only on the eigenvalue error, is employed; see Table 4.2. In this case we see an improvement of the effectivities for the full error indicator in comparison to the previous example; in this case the effectivities tend to unity in much fewer refinement steps, this possibly being due to

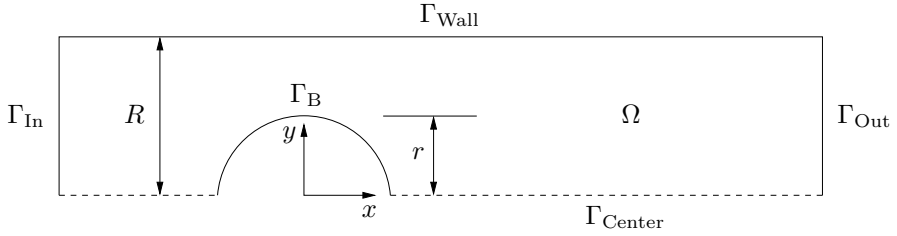

FIG. 4.5. *Example 2: Half Channel with a Cylindrical Blockage*

Mesh No	No. Eles	Base DOF	Eig. Dof	$\lvert\lambda - \lambda_h\rvert$	$\lvert\sum_{\kappa\in\mathcal{T}_h} \hat{\eta}_\kappa\rvert$	$\lvert\sum_{\kappa\in\mathcal{T}_h} \hat{\eta}^m_\kappa\rvert$
1	816	17952	17952	8.966E-02	1.08	4.51E-02
2	1443	31746	31746	2.229E-03	1.54	0.55
3	2577	56694	56694	1.455E-04	1.31	0.68
4	4590	100980	100980	4.089E-05	0.98	0.53
5	8190	180180	180180	1.033E-05	1.01	0.81
6	14400	316800	316800	3.870E-06	0.95	0.51
7	24843	546546	546546	1.060E-06	1.00	0.97

TABLE 4.2
Example 2: Convergence and Effectivities

greater regularity of the dual base and eigenvalue problems. Once again, the partial error indicators prove unreliable, consistently underestimating the error; however, on the final grid the partial error indicator effectivity is quite reasonable. Evidently, if the primal base solution is completely resolved, then the partial and full error indicators will both provide a reliable estimates for the size of the discretization error in the computed eigenvalue.

Figures 4.6(a) and (b) show the adaptively refined mesh after 6 refinement steps, the former showing the full extent of the mesh, while the latter shows the mesh detail near to the blockage. We notice that the majority of refinement has been performed downstream of the blockage, with substantially less being undertaken upstream. Figure 4.6(c) shows a contour plot of the y–component of the dual base solution $\mathbf{z}^0$ over the same portion of the domain as depicted in Figure 4.6(b). It can be seen that some of the mesh refinement in the right portion of the domain has been carried out in response to the fine structures present in the dual base solution.

Finally, we again compare the error in the computed eigenvalue, using our adaptive refinement strategy, with that using uniform refinement, see Figure 4.7. The adaptive refinement strategy shows a marked improvement over the uniform refinement strategy; indeed, on the final grid the adaptive refinement strategy shows over an order of magnitude improvement in error for the same number of degrees of freedom as the uniform strategy.

4.3. Example 3. In this final example we consider a cylindrical pipe, of radius R, blocked by a sphere, of radius r, centered on the axis of symmetry of the pipe. Here, we shall be interested in an axisymmetric steady solution and hence we can use the same two–dimensional domain as shown in Figure 4.5 to calculate the base flow; once again we choose $R : r = 2 : 1$. This symmetric steady solution is known to be unstable for $Re \approx 360$, hence we pick $Re = 350$ and seek to adapt the mesh to locate the smallest real eigenvalue. We use the techniques developed in [10] in order to only

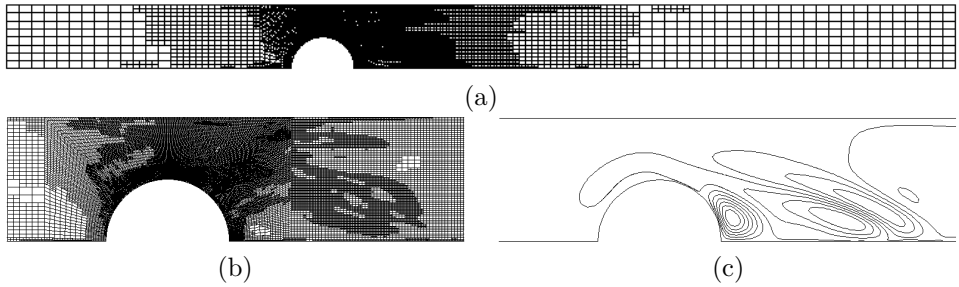

FIG. 4.6. *Example 2: (a) Final mesh, (b) Mesh detail near blockage, (c) Contour plot of* $\mathbf{z}_y$ *near blockage.*

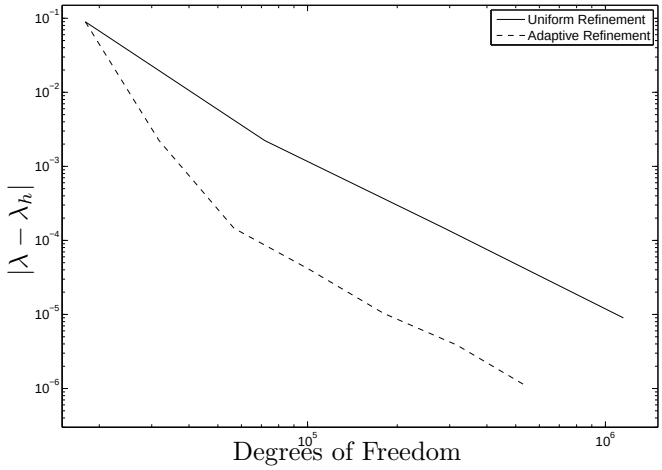

FIG. 4.7. *Example 2: Error Convergence*

consider a two–dimensional analogue of the problem, albeit with an extra azimuthal component for the velocity vector. The true eigenvalue is 0.015358133759879. As before, we use an initial mesh fitted to the blockage, this time with 1016 elements and carry out adaptive refinement using the fixed fraction refinement strategy.

Table 4.3 shows the effectivities for the full and partial error indicators, $|\sum_{\kappa\in\mathcal{T}_h}\hat{\eta}_\kappa|$ and $|\sum_{\kappa\in\mathcal{T}_h}\hat{\eta}^m_\kappa|$, respectively. Again, the full error indicators have effectivities settling down to 1 after only 2 refinement steps. In contrast, the effectivities computed employing only the partial error indicators for the eigenproblem alone tend to oscillate around unity, thereby indicating that reliable estimates for the true error in the computed eigenvalue cannot be inferred from this quantity.

In Figures 4.8(a) and (b) we show the adapted mesh after 4 refinement steps; the first shows the whole of the computational domain, while the second shows the mesh detail near the blockage. As with the blocked channel, the majority of mesh refinement is seen to be carried out slightly downstream of the blockage with significantly less refinement of the mesh undertaken upstream of the blockage. Figure 4.8(c) shows the radial component of the dual base solution $\mathbf{z}^0_r$ on the same portion of the domain depicted in Figure 4.8(b). Once again, we observe that the mesh in the right portion

Mesh No	No. Eles	Base DOF	Eig. Dof	$\lvert\lambda - \lambda_h\rvert$	$\lvert\sum_{\kappa\in\mathcal{T}_h}\hat{\eta}_\kappa\rvert$	$\lvert\sum_{\kappa\in\mathcal{T}_h}\hat{\eta}^m_\kappa\rvert$
1	1016	22352	31496	1.384E-01	1.68	.114E-01
2	1793	39446	55583	2.552E-03	2.01	2.70
3	3158	69476	97898	4.877E-04	0.94	0.67
4	5624	123728	174344	2.467E-05	1.02	1.14
5	10301	226622	319331	2.111E-06	1.08	2.69

TABLE 4.3
Example 3: Convergence and Effectivities

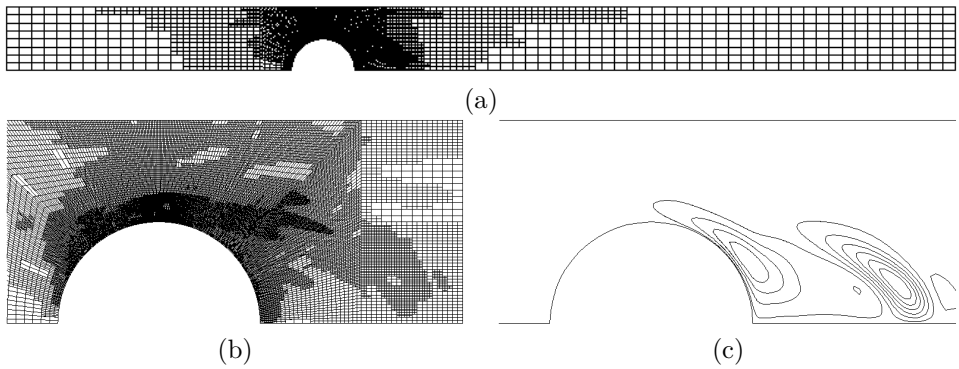

FIG. 4.8. *Example 3: (a) Final mesh, (b) Mesh detail near blockage, (c) Contour plot of* $\mathbf{z}_r^0$ *near blockage.*

of the visible domain has been refined in response to the fine structures present in $\mathbf{z}_r^0$; indeed, no other component of the solution exhibits these same features.

Finally, Figure 4.9 gives a comparison of the error in the computed eigenvalue employing both the proposed adaptive refinement strategy and uniform mesh refinement. As with the previous examples, the adaptive strategy shows a great improvement in the error in the computed eigenvalue in comparison to the same quantity computed using uniform refinement; indeed, on the final mesh, we witness over two orders of magnitude improvement in error when the adaptive strategy is employed.

5. Concluding remarks. In this article we have considered the *a posteriori* error estimation and adaptive mesh refinement of discontinuous Galerkin approximations of the hydrodynamic stability problem associated with the incompressible Navier–Stokes equations. In particular, by constructing both a dual eigenvalue problem and a dual problem for the original base solution, an *a posteriori* error estimator has been derived based on employing a generalization of the standard DWR approach, originally developed for the estimation of target functionals of the solution, to eigenvalue/stability problems. In this way, errors stemming from both the numerical approximation of the original nonlinear flow problem, as well as the underlying linear eigenvalue problem are correctly controlled. Indeed, numerical experiments presented in this article clearly demonstrate that the resulting error indicators lead to reliable estimation of the underlying eigenvalue of interest: as the mesh is refined the computed effectivity indices tend to unity. In contrast, the quality of the error indicator significantly deteriorates if the error related to the discretization of the original base flow is neglected in the analysis. The application of these techniques to the reliable approximation of bifurcation problems is in progress and will be reported elsewhere.

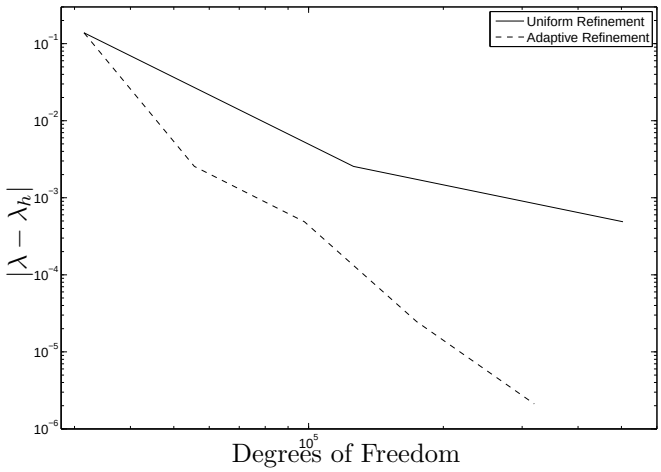

FIG. 4.9. *Example 3: Error Convergence*

REFERENCES

[1] M. Ainsworth and J.T. Oden. *A Posteriori Error Estimation in Finite Element Analysis.* Series in Computational and Applied Mathematics. Elsevier, 1996.

[2] P.R. Amestoy, I.S. Duff, and J.-Y. L'Excellent. Multifrontal parallel distributed symmetric and unsymmetric solvers. *Comput. Methods Appl. Mech. Engrg.*, 184:501–520, 2000.

[3] D.N. Arnold, F. Brezzi, B. Cockburn, and L.D. Marini. Unified analysis of discontinuous Galerkin methods for elliptic problems. *SIAM J. Numer. Anal.*, 39:1749–1779, 2001.

[4] I. Babuška and J. Osborn. A posteriori error estimates for the finite element method. *Internat. J. Numer. Methods Engrg.*, 12:1597–1615, 1978.

[5] I. Babuška and Tsuchiya. A posteriori error estimates of the finite element solutions of parameterized nonlinear equations. Technical report, University of Maryland, 1992.

[6] W. Bangerth and R. Rannacher. *Adaptive Finite Element Methods for Differential Equations (Lectures in Mathematics, ETH Zurich).* Birkhauser Verlag AG, 2003.

[7] R. Becker and R. Rannacher. An optimal control approach to a-posteriori error estimation in finite element methods. In A. Iserles, editor, *Acta Numerica*, pages 1–102. Cambridge University Press, 2001.

[8] K.A. Cliffe, T.J. Garratt, and A. Spence. Eigenvalues of the discretized Navier-Stokes equations with application to the detection of Hopf bifurcations. *Adv. Comp. Math.*, 1:337–356, 1993.

[9] K.A. Cliffe, E. Hall, and P. Houston. Adaptivity and a posteriori error control for bifurcation problems I: The Bratu problem. In preparation.

[10] K.A. Cliffe, A. Spence, and S.J. Tavener. O(2)-symmetry breaking bifurcation: with application to the flow past a sphere in a pipe. *Internat. J. Numer. Methods Fluids*, 32:175–200, 2000.

[11] K.A. Cliffe and S.J. Tavener. The effect of cylinder rotation and blockage ratio on the onset of periodic flows. *J. Fluid Mech.*, 501:125–133, 2004.

[12] B. Cockburn, G. Kanschat, and D. Schötzau. The local discontinuous Galerkin method for the Oseen equations. *Math. Comp.*, 73:569–593, 2004.

[13] B. Cockburn, G. Kanschat, D. Schötzau, and C. Schwab. Local discontinuous Galerkin methods for the Stokes system. *SIAM J. Numer. Anal.*, 40:319–343, 2002.

[14] R.G. Durán, L. Gastaldi, and C. Padra. A posteriori error estimators for mixed approximations of eigenvalue problems. *Math. Models Methods Appl. Sci.*, 9:1165–1178, 1999.

[15] R.G. Durán, C. Padra, and R. Rodriguez. A posteriori error estimates for the finite element approximation of eigenvalue problems. *Math. Models Methods Appl. Sci.*, 13(8):1219–1229, 2003.

[16] K. Eriksson, D. Estep, P. Hansbo, and C. Johnson. Introduction to adaptive methods for differential equations. In A. Iserles, editor, *Acta Numerica*, pages 105–158. Cambridge University Press, 1995.

[17] R.M. Fearn, T. Mullin, and K.A. Cliffe. Nonlinear flow phenomena in a symmetric sudden expansion. *J. Fluid Mech.*, 211:595–608, 1990.

[18] T.J. Garratt. *The numerical detection of Hopf bifurcations in large systems arising in fluid mechanics*. PhD thesis, University of Bath, 1991.

[19] S. Giani and I. Graham. A convergent adaptive method for elliptic eigenvalue problems. Submitted for publication.

[20] P. Hansbo and M.G. Larson. Discontinuous finite element methods for incompressible and nearly incompressible elasticity by use of Nitsche's method. *Comput. Methods Appl. Mech. Engrg.*, 191:1895–1908, 2002.

[21] V. Heuveline and R. Rannacher. A posteriori error control for finite element approximations of elliptic eigenvalue problems. *Adv. Comp. Math.*, 15:107–138, 2001.

[22] P. Houston and E. Süli. Adaptive finite element approximation of hyperbolic problems. In T. Barth and H. Deconinck, editors, *Error Estimation and Adaptive Discretization Methods in Computational Fluid Dynamics. Lect. Notes Comput. Sci. Engrg.*, volume 25, pages 269–344. Springer, 2002.

[23] M.G. Larson. A posteriori and a priori error analysis for finite element approximations of self–adjoint elliptic eigenvalue problems. *SIAM J. Numer. Anal.*, 38:608–625, 2000.

[24] M.G. Larson and T.J. Barth. A posteriori error estimation for discontinuous Galerkin approximations of hyperbolic systems. In B. Cockburn, G.E. Karniadakis, and C.-W. Shu, editors, *Discontinuous Galerkin Methods: Theory, Computation and Applications, Lecture Notes in Computational Science and Engineering, Vol. 11*. Springer, 2000.

[25] R.B. Lehoucq, D.C. Sorensen, and C. Yang. *ARPACK USERS GUIDE: Solution of Large Scale Eigenvalue Problems by Implicitly Restarted Arnoldi Methods*. SIAM, Philadelphia, PA, 1998.

[26] C. Lovadina, M. Lyly, and R. Stenberg. A posteriori estimates for the Stokes eigenvalue problem. *Num. Meth. Part. Diff. Eqs.* In Press.

[27] C. Nystedt. A priori and a posteriori error estimates and adaptive finite element methods for a model eigenvalue problem. Technical Report 1995-05, Chalmers Finite Element Center, Chalmers University, 1995.

[28] P. Schmid and D. S. Henningson. *Stability and Transition in Shear Flows*. Applied Mathematical Sciences. Springer-Verlag, 2001.

[29] D. Schötzau, C. Schwab, and A. Toselli. Mixed *hp*-DGFEM for incompressible flows. *SIAM J. Numer. Anal.*, 40:2171–2194, 2003.

[30] K. Shahbazi, P.F. Fischer, and C.R. Ethier. A high-order discontinuous Galerkin method for the unsteady incompressible Navier–Stokes equations. *J. Comput. Phys.*, 222(1):391–407, 2007.

[31] B. Szabó and I. Babuška. *Finite Element Analysis*. J. Wiley & Sons, New York, 1991.

[32] A. Toselli. *hp*-Discontinuous Galerkin approximations for the Stokes problem. *Math. Models Methods Appl. Sci.*, 12:1565–1616, 2002.

[33] R. Verfürth. A posteriori error estimates for nonlinear problems. *Math. Comp.*, 62:445–475, 1989.

[34] R. Verfürth. *A Review of a Posteriori Error Estimation and Adaptive Mesh-Refinement Techniques*. B.G. Teubner, Stuttgart, 1996.

[35] T.F. Walsh, G.M. Reese, and U.L. Hetmaniuk. Explicit a posteriori error estimates for eigenvalue analysis of heterogeneous elastic structures. *Comput. Methods Appl. Mech. Engrg.*, 196:3614–3623, 2007.

[36] B. Werner and A. Spence. The computation of symmetry-breaking bifurcation points. *SIAM J. Numer. Anal.*, 21:388–399, 1984.